

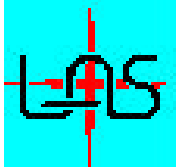
## Integral Field / Multi-Object Spectrograph for the NGST

ESA Contract: 13003/98/NL/MS



ESA Study Manager: J. Cornelisse

Prepared by : **Olivier Le Fèvre and the IFMOS Consortium**

 CNRS	 DaimlerChrysler Aerospace Dornier Dornier Satellitensysteme GmbH	 University of Durham		
				

## TABLE OF CONTENTS

<b>1</b>	<b>EXECUTIVE SUMMARY.....</b>	<b>5</b>
<b>2</b>	<b>INTRODUCTION .....</b>	<b>6</b>
<b>3</b>	<b>IFMOS STUDY TEAM.....</b>	<b>7</b>
<b>4</b>	<b>SCIENCE.....</b>	<b>7</b>
4.1	ASTROPHYSICAL RATIONALE .....	7
4.2	SCIENTIFIC PROGRAM FOR THE SPECTROGRAPH.....	7
4.3	REQUIRED OPERATING MODES .....	16
4.4	INTEGRAL FIELD SPECTROSCOPY VS. MULTI-SLIT SPECTROSCOPY .....	16
<b>5</b>	<b>CONCEPT REVIEW – TRADE-OFF ANALYSIS.....</b>	<b>17</b>
5.1	REVIEW OF POSSIBLE CONCEPTS .....	17
5.2	SUITABILITY ASSESSMENT.....	18
5.3	TECHNICAL SPECIFICATIONS.....	19
<b>6</b>	<b>DESIGN OVERVIEW .....</b>	<b>19</b>
6.1	INSTRUMENT DESIGN.....	19
6.2	DESIGN TRADES.....	21
<b>7</b>	<b>OPTICAL DESIGN DESCRIPTION.....</b>	<b>21</b>
7.1	DESIGN DRIVERS .....	21
7.2	MAIN SUBSYSTEMS.....	22
7.3	OVERALL IMPLEMENTATION: .....	24
<b>8</b>	<b>IMAGE SLICER OPTICAL DESIGN .....</b>	<b>25</b>
8.1	OPTICAL PRINCIPLE .....	25
8.2	DESIGN ISSUES .....	27
8.3	DETAILED OPTICAL DESCRIPTION.....	27
8.4	SUMMARY OF SLICER OPTICAL DESIGN .....	29
8.5	PRODUCTION ISSUES .....	29
8.6	ESTIMATED THROUGHPUT OF INTEGRAL FIELD UNIT .....	31
8.7	REFERENCES.....	31
<b>9</b>	<b>SPECTROGRAPH OPTICAL DESIGN .....</b>	<b>32</b>
9.1	OVERALL PRESENTATION .....	32
9.2	LOW RESOLUTION CHANNEL.....	32
9.3	HIGH RESOLUTION SPECTROGRAPH.....	33
<b>10</b>	<b>PERFORMANCE EVALUATION.....</b>	<b>35</b>
10.1	DESIGN PERFORMANCE .....	35
10.2	EXPOSURE TIME CALCULATOR, LIMITING MAGNITUDES .....	35
10.3	PERFORMANCE SIMULATION: OBSERVING FAINT DISTANT GALAXIES FROM THE HUBBLE DEEP FIELD NORTH WITH NGST-IFMOS LR MODE.....	36
10.4	OVERALL EFFICIENCY .....	38
<b>11</b>	<b>MECHANICAL, THERMAL AND ELECTRICAL DESIGN AND ANALYSIS.....</b>	<b>41</b>
11.1	INTRODUCTION.....	41
11.2	MECHANICAL DESIGN AND ANALYSIS .....	41
11.3	THERMAL DESIGN AND ANALYSIS .....	46
11.4	ELECTRICAL DESIGN AND ANALYSES.....	48
11.5	TECHNICAL BUDGETS SUMMARY .....	51
<b>12</b>	<b>CRITICAL AREAS, DEVELOPMENT NEEDS AND FOLLOW-ON ACTIVITIES.....</b>	<b>51</b>

12.1	CRITICAL AREAS AND TECHNOLOGY REQUIREMENTS .....	51
12.2	RECOMMENDED FOLLOW-ON ACTIVITIES .....	55
<b>13</b>	<b>DEVELOPMENT PLANNING FOR PHASE B AND C/D .....</b>	<b>57</b>
13.1	WORK BREAKDOWN STRUCTURE .....	57
13.2	DEVELOPMENT PLANNING .....	57
<b>14</b>	<b>SUMMARY AND CONCLUSIONS.....</b>	<b>62</b>

## LIST OF FIGURES

Figure 1:	The star formation history of the universe (from Baugh et al., 1998, ApJ, 498, 504).....	10
Figure 2:	Integral Field Spectroscopy of ( <i>left</i> ) the core of M31, ( <i>right</i> ) a QSO and companion at $z=4.7$ (CFHT and Tiger).....	13
Figure 3:	The dynamical study of a lensed galaxy with $z=1.018$ from Argus spectroscopy (Soucail et al 1999)....	15
Figure 4:	A possible example of galaxy-galaxy lensing in the HDF following Hogg et al (1996). The 16 possible components of a distant image lie within a 5 arcsec field. The spectroscopic study of more distant and fainter examples is ideally suited to a IFU. ....	15
Figure 5 :	Integral field spectroscopy possible concepts.....	18
Figure 6 :	Low resolution channel concept.....	20
Figure 7 :	high resolution channel concept.....	20
Figure 8:	IFMOS Field of View .....	23
Figure 9 :	overall optical layout , Low resolution channel is on the left (one of 3 modules shown), the High resolution channel is on the right.....	24
Figure 10 :	Principle of Advanced Image Slicer .....	26
Figure 11:	HR fore-optics layout. The three mirrors of the fore-optics are labeled F1, F2 and F3. The slicing mirror is indicated by S1.....	27
Figure 12 :	HR mode spot diagrams at S1 over the full field. The box size is the width of the slice.....	27
Figure 13:	HR slicing unit. Rays from two slices are shown .....	28
Figure 14:	HR mode spot diagrams at S3 (the slit) for the central slice for different positions along the slice. The box size is equivalent to 2 pixels on the detector .....	28
Figure 15:	LR fore-optics (fore-optics mirrors = F1, F2; slicing mirror S1). S1' indicates the second of each pair of slicing mirrors feeding a single spectrograph. ....	28
Figure 16:	LR mode spot diagrams at S1 over the full extent of the central subfield. The box size is equal to the width of a slice.....	28
Figure 17:	Layout of LR slicing unit. Paths from two slices at the slicing mirror (S1) are shown. S2 and S3 are the pupil and slit mirrors respectively. ....	29
Figure 18:	LR mode spot diagrams for one slice at S3 (the slit) over the length of the slice. The results for all the slices is very similar. The box size is 1 pixel.....	29
Figure 19:	Illustration of Proof of Concept. Left: layout on the vacuum chuck which allows arbitrary figures of rotation to be generated. Centre: definition of the centre of curvature of the spherical surface. Right: picture of assembled POC.....	30
<b>Figure 20:</b>	<b>Picture of POC slices on the vacuum chuck at POE. The diamond tool can be seen at the extreme right.....</b>	<b>31</b>
Figure 21:	overview of one low resolution spectrograph .....	32
Figure 22:	LR Collimator .....	33
Figure 23:	LR camera .....	33
Figure 24:	Image quality at the field center (circle=18microns) .....	34
Figure 25:	Side view of the HR spectrograph.....	34
Figure 26 :	image quality with the HR spectrograph (circle = 18 microns).....	34
Figure 27 :	part of the HDF North with IFMOS sampling (0.19 arcsec) and field of view (40x46 arcsec <sup>2</sup> ).....	37
Figure 28 :	A simulated LR long exposure (10x1000 s) of the HDF north. For each pixels shown in that figure the corresponding spectrum has a S/N larger than 5 by spectral elements. Blue pixels : original resolving power (R=150, 200 spectral elements). Green pixels : coaddition of 5 spectral .....	37
Figure 29:	Spectral resolution and limiting magnitude. Left panel : limiting surface AB magnitude (S/N=5 in 10 exposure of 1000s) as function of the resolving power. Right panel: Number of active pixels (with a S/N > 5) in the corresponding exposure.....	38

Figure 30 : geometric limitation of a multi-slit spectrograph preventing from getting spectra of all objects in a field at once. This limitation forces to multiply the number of slit settings until all objects of interest have been observed, hence with an overall efficiency divided by the number of slit settings .....	40
Figure 31 : galaxies with AB~28-29 have half light radii on order 0.1 arcsec. A 0.1 arcsec slit introduces light losses of ~1/2 the total flux. An integral field spectrograph does not lose any light and allows to use optimal extraction techniques to maximize the S/N. Longer exposure times are thus required for a MOS to reach the same S/N as an IFS. A MOS could have slits with 0.2 arcsec width, but this will compromise the spectral resolution, or the field of view. ....	40
Figure 32 : opto-mechanical implementation of the optical design (top plate taken off) .....	43
Figure 33 : complete instrument with view on HR spectrograph .....	43
Figure 34 : top view of LR spectrograph showing the vertical panels .....	44
Figure 35 : principle of mirror light-weighting and mirror mounting .....	44
Figure 36 : normal mode 1 (69.7 Hz) .....	45
Figure 37 : Thermal Design Concept for IFMOS Detector Cooling .....	47
Figure 38: Functional Block Diagram .....	49
Figure 39: Power Budget and Harness Size .....	50
Figure 40 : Instrument Hardware Breakdown, indicating critical subsystems .....	52
Figure 41 : IFMOS Technology Development Roadmap .....	55
Figure 42 : Function oriented Work Breakdown Structure .....	57
Figure 43 : Standard Model Philosophy .....	58
Figure 44 : Proposed Development Schedule for Standard Model Philosophy .....	59
Figure 45: Alternative Model Philosophy .....	60
Figure 46: Proposed Development Schedule for the Alternative Model Philosophy .....	61

## LIST OF TABLES

Table 1 : The IFMOS Design Reference Mission .....	8
Table 2: science requirements .....	16
Table 3 : Concept suitability assessment .....	18
Table 4 : IFMOS Technical Specifications .....	19
Table 5 : Design performance summary .....	22
Table 6 : HR mode summary .....	25
Table 7 : LR mode summary .....	25
Table 8 : integral field unit throughput .....	31
Table 9: Prisms Characteristics .....	33
Table 10 : performances advantages .....	35
Table 11 : IFMOS limiting magnitude .....	36
Table 12 : parameters entering efficiency comparisons between spectrograph concepts .....	39
Table 14: maximum VON MISES stresses in the primary structure due to static acceleration loads .....	46
Table 15 : mass budget .....	46
Table 16: IFMOS Detector Requirements .....	48
Table 17: Instrument budget summary .....	51
Table 18 : Potential critical areas of the IFMOS spectrograph .....	53

## 1 EXECUTIVE SUMMARY

This report presents the results from the NGST study for an integral field / multi-object spectrograph (IFMOS) conducted under contract with ESA by a consortium of 7 leading European astronomical institutes teaming up with Dornier Satellittensysteme GmbH.

In the initial phase of the study, we reviewed the science requirements, and then conducted a trade-off analysis of several competing concepts. Based on this trade-off, we concluded that the approach of *integral field (3D) spectroscopy* is not only particularly well suited to the NGST science objectives but also offers significant technical and operational advantages.

One of the key drivers for near-infrared spectroscopy with NGST is the ability to observe a large number of sources simultaneously, while preserving the superb image quality of a space observatory. At the limiting magnitudes foreseen, most astrophysical fields from nearby galaxies to the most distant primeval objects, require observing large samples from which statistical studies can be efficiently conducted. In addition, the measurement of two dimensional fields like velocity, abundance, line intensity, etc., are required to understand the complex physical conditions at play. Integral field spectroscopy allows the science programs identified so far for NGST to be conducted with high efficiency, while maintaining great flexibility for other future types of observations.

Recent advances in the field of integral field spectroscopy allow one to design a spectrograph with wide field survey capabilities combined with highly detailed spectroscopic mapping at the diffraction limit of the NGST. The spectrograph design presented here offers two observing modes, *both of these modes being available simultaneously*:

- The first observing mode, the *Low Resolution mode* (survey mode), offers a field of 46x40 arcseconds, and a spectral resolution  $R \sim 150$ . Three small spectrograph units are fed by an image slicer unit. Each 0.19x0.19 square arcsecond elements on the sky yields a critically sampled spectrum on the detector, thus providing a full 3D integral field spectrograph capability. Each spectrograph has a blue and a red channel to cover the 1.25-5.μm domain in a single exposure.
- The second observing mode, the *High Resolution mode*, offers a 3.8x2.6 arcseconds field, sampled at 0.05 arcsecond, and a spectral resolution of  $R \sim 3000$ . A single spectrograph unit covers one octave in wavelength at a time for each 0.05x0.05 square arcsecond sky elements in the field.

During the detailed design phase, we have taken great care to produce a realistic design in terms of optical design, payload environment constraints, mechanisms, and ease of operation. The optical elements employed are easy to manufacture, and we have taken great care to minimize diffraction losses, a parameter often underestimated in spectrographs using small entrance apertures. The most critical items are the image slicers: expanding from our ground experience, we have successfully conducted a proof of concept study, and a detailed prototype slicer is being manufactured. The total weight of the complete instrument is less than ¼ of the full payload allocation, and the power consumption is within the allocated budget. IFMOS contains only one moving part: a simple grating exchange mechanism in the HR channel. Operations are extremely simple, akin to conventional cameras, requiring only "point and shoot" type target acquisition.

The single source sensitivity of IFMOS is comparable to that of a slit spectrograph in the case of point sources. However, since there are no slit losses, the limiting sensitivity is better for extended objects. IFMOS offers superb multi-object capabilities: all sources in even the most crowded fields can be observed down to the faintest magnitudes in a single pointing without needing to worry about overlap of spectra.

## 2 INTRODUCTION

Spectroscopy with the NGST in the 1 to 5 microns domain is considered to be one of the core requirements for the mission [ref.1]. NGST will have a fixed payload, without any possibility to upgrade the instrument suite during the life of the spacecraft. Selecting a particular instrument concept therefore requires to balance the instrument performances compared to all science projects already identified, e.g. in the Design Reference Mission (DRM), or all future programs to be conducted with the instruments 10 years from now, and for a period of about 10 years. This is a notoriously difficult exercise, but these constraints force one to explore versatile instrument concepts with great versatility, able to cope with the most complex science requirements now and then.

Following the report from the ESA-NGST Task Group [ref.2], and as a step to define its participation in the NGST project, ESA has launched in May 1998 an invitation to tender (AO/1-3405/98/NL/MS) for an integral field / multi-object spectrograph in the 1-5 microns domain. Our consortium, led by the *Laboratoire d'Astronomie Spatiale* in Marseilles, France, was subsequently selected to conduct this study.

Based on a trade-off analysis, we have selected the concept of integral field (3D) spectroscopy as the most appropriate in the NGST context. Integral field spectroscopy is a relatively novel concept, now introduced at most major ground based observatories. European teams have been leading developments in this field, and members of our consortium have been delivering and are manufacturing facility class instruments to be used at several sites.

This report presents the results of the study. Section 4 presents the science requirements, followed by a concept trade-off analysis in Section 5. The optical design is presented in Sections 7 to 9. Overall performances are described in Section 10. The mechanical, thermal and electrical design is presented in Section 11.

The final presentation of the results of this study took place June 17<sup>th</sup>, 1999 at ESTEC.

### References

1. Stockman, P., The Next Generation Space Telescope - Visiting a time when galaxies were young, Edited by H.S. Stockman, STScI, June 1997 (<http://opposite.stsci.edu/ngst/initial-study>)
2. Next Generation Space Telescope, Report from the NGST Task Group, ESA, October 1997 (available at <http://astro.estec.esa.nl/NGST/>)

### 3 IFMOS STUDY TEAM

Our consortium brings together experts in the field of observational cosmology and extragalactic astronomy, multi-slit and integral field spectroscopy, and the space engineering experience of one of the largest European space company. Some of us are, in particular, building the GMOS multi-slit and integral field spectrograph for Gemini (Allington-Smith et al., 1998, SPIE, 3354), the VIMOS and NIRMOS multi-slit and integral field spectrographs for the VLT (Le Fèvre et al., 1998, SPIE, 3354), the SINFONI integral field spectrograph for the VLT (Thatte et al., 1998, SPIE, 3354).

Key study team personnel:

- . *O. Le Fèvre*, Principal Investigator, Laboratoire d'Astronomie Spatiale, Marseille, France
- . *E. Prieto*, Study Manager, Laboratoire d'Astronomie Spatiale, Marseille, France
- . *W. Posselt*, DSS Project Manager, coordinating the DSS team (key DSS personnel see §11.1), Dornier SatellitenSysteme GmbH, Ottobrun, Germany
- . *R. Bacon*, co-Investigator, Lyon Observatory, France
- . *R. Davies*, co-investigator, Durham University, UK
- . *R. Ellis*, co-investigator, Institute of Astronomy Cambridge, UK
- . *G. Monnet*, co-Investigator, European Southern Observatory, Garching, Germany
- . *N. Thatte*, co-investigator, Max Planck Institute für Extraterrestrische Physik, Garching, Germany
- . *T. de Zeeuw*, co-investigator, Leiden Observatory, the Netherlands
- . *J. Allington-Smith*, Durham study coordinator, Durham University, UK
- . *B. Delabre*, optical engineer, European Southern Observatory, Garching, Germany
- . *R. Content*, optical designer, Durham University, UK

### 4 SCIENCE

#### 4.1 ASTROPHYSICAL RATIONALE

This study fits within the overall science frame of the NGST mission. The Design Reference Mission (DRM) details the overall science objectives. We have explored:

- . Which fraction of the DRM will (should) be addressed by the IFMOS concept
- . The science areas which are not covered by the DRM, which are nevertheless of importance to scientists in Europe

#### 4.2 SCIENTIFIC PROGRAM FOR THE SPECTROGRAPH

##### 4.2.1 Science cases

We have identified 4 science cases in our proposal:

- . Evolution of galaxies beyond  $z=2$
- . Large scale structures, clustering, proto-clusters
- . Evolution of the morphology and dynamics of galaxies
- . Strong and weak lensing

These science cases have been used to revisit the DRM, and to identify in the DRM those areas which should be addressed by the spectrograph. Several science areas are listed in Table 1. Most of the programs are now listed in the new DRM, although the emphasis on galaxy clustering, and the study of galaxies in clusters, is quite limited at present.

**Table 1 : The IFMOS Design Reference Mission**

Program	Spectral Range	Inst	SNR	Spectral Res.	V Mag	Size Arcsec	Density /arcmin <sup>2</sup>	Required Number	Visits
<i>COSMIC DISTANCES - CORE</i>									
SN spectro	1-5	NIRS	3	100	28.5	0	0	100	1
<i>UNIVERSE AT z&gt;2 - CORE</i>									
Prim Gal. Spectro -deep	0.6-5	NIRS	10	100	28.0	.5	1000	9000	1
Prim Gal. Spectro -shallow	1-5	NIRS	10	100	25.5	.5	300	270000	1
Prim. Gal. Spectro high res	1-5	NIRS	10	1000	25.5	.5	300	2700	1
Prim. Gal. Spectro high res	1-5	NIRS	10	1000	24.5	.5	100	9000	1
Prim. Gal. Spectro high res	1-5	NIRS	10	1000	23.5	.5	60	5400	1
<b>Gravitational lensing</b>	<b>1-5</b>	<b>NIRS</b>	<b>100</b>	<b>200-3000</b>	<b>28.0</b>	<b>.2</b>	<b>0</b>	<b>TBD</b>	<b>1</b>
<b>Cluster spectro deep</b>	<b>1-5</b>	<b>NIRS</b>	<b>10</b>	<b>1000</b>	<b>28.0</b>	<b>.5</b>	<b>3000</b>	<b>TBD</b>	<b>1</b>
<b>Cluster spectro shallow</b>	<b>1-5</b>	<b>NIRS</b>	<b>10</b>	<b>1000</b>	<b>25.5</b>	<b>.5</b>	<b>1000</b>	<b>TBD</b>	
<b>Large Scale Structure spectro</b>	<b>1-5</b>	<b>NIRS</b>	<b>10</b>	<b>200-3000</b>	<b>28.0</b>	<b>.5</b>	<b>1000</b>	<b>TBD</b>	<b>1</b>
<b>Galaxies dynamics</b>	<b>1-5</b>	<b>NIRS</b>	<b>10</b>	<b>5000</b>	<b>25.5</b>	<b>.5</b>	<b>300</b>	<b>TBD</b>	<b>1</b>
<b>Chemical evolution</b>	<b>1-5</b>	<b>NIRS</b>	<b>10</b>	<b>3000</b>	<b>25.5</b>	<b>.5</b>	<b>300</b>	<b>TBD</b>	<b>1</b>
<i>UNIVERSE AT z&gt;2 - COMPL</i>									
Birth quasars spectro	2-3	NIRS	5	200-3000	28.5	0.0	0	30	1
Primeaval spheroids	3-5	NIRS	5	200-3000	27	.5	0.02	150	1
Evolution of disks	3-5	NIRS	60	200-3000	24	1.0	0.02	50	1
Early evol of galaxies		NIRS	10	200-3000	26.5	0.5	0.02	150	1
Origin of ISM	0.8-5	NIRS	5	100	26	1.0	0	50	1
<i>CHEMICAL EVOLUTION OF ISM</i>	0.5-5	NIRS	30	1000	22	0.	0	150	1
<i>ACTIVE GALAXIES</i>									
Spectroscopy NIR	1-5	NIRS	5	1000	25	0.1	0	100	1
<i>STELLAR POPULATION</i>									
Local Group study	0.5	NIR	10	5	28.7	0	0	150	1
Virgo Cluster study	0.5	NIR	10	5	30.2	0	0	15	1

#### 4.2.1.1 Science case no.1: Evolution of galaxies beyond z=2

It is believed that galaxy formation proceeded hierarchically, so that slowly, through gravitational instability, the spectacular galaxies we see around us today were built from the small fragments we observe at high redshift. The process of galaxy formation extends over many billions of years and the goal of studies of galaxy evolution is to chart each stage of that process to generate a clear picture of how and when typical galaxies were assembled. How did the faint wisps we see in the Hubble Deep Field come to be and how did they evolve into present day galaxies?

The combination of the Hubble Space Telescope and large ground based telescopes has produced a picture of how this process works in reasonable detail out to z=0.5-1.0. At that epoch, about 4-7 Gyrs ago, spiral galaxies were more common in rich clusters than they are today (Dressler et al 1998) and in the field blue star-forming galaxies were much more common (Lilly et al 1996). Extending our study of galaxies to higher redshifts (z=2-3) in the Hubble Deep Field, Madau et al. 1996, and further studies have been able to estimate the rate of star formation in the universe as a function of redshift. As

Figure 1 shows the star formation rate rises sharply back to  $z=1$  reaching a broad peak with a flattening or declining rate for  $z>2$ . This is within the predicted range of cosmological simulations based on semi-analytic galaxy evolution models in a hierarchical clustering cosmology (Baugh et al 1996). However at around  $z=2$  our view of galaxies becomes buried in the infrared background that prevails from the ground and the well established diagnostics of star formation rate, age and metallicity of galaxies pass into the near infrared spectral region that is sliced up by the transmission of the earth's atmosphere. HST's NICMOS has provided a preliminary view of this spectral region but lacks both the sensitivity and resolution to probe to  $z>2$  that will be the forte of NGST.

The infrared spectroscopy with NGST will probe galaxies in the first 3-4 billion years of galaxy evolution. In this interval we expect the oldest star clusters to form, the bulk of the chemical elements and therefore cosmic dust to be created, and the sites for the formation of luminous galaxies to be established. Paradoxically our diagnostics of the age of the integrated light of stellar populations are more sensitive and more accurate for populations that are less than 3-4 Gyrs old than they are for the local 10-15 Gyr old populations. We therefore expect to be able to determine the ages and metallicities of these pre-galactic fragments once NGST measures their spectral energy distributions. We expect the tight correlation between present day local galaxy density and the mix of galaxy morphological types observed today, to be seeded as early fragments coalesce to create the precursors of present day clusters and groups of galaxies. A redshift survey to faint limits by NGST will establish which high redshift wisps are physically associated and determine their gas content and star formation rate through the increasingly evident H-alpha and OII emission lines. We will be able explore the relationship between size, brightness, metallicity, age and star formation rate as a function of redshift and local density. Large samples are required to reach a satisfactory level of accuracy.

Integral field spectroscopy will play a critical role in testing hierarchical models for the formation of galaxies by measuring the mass of fragments as a function of redshift. By sampling galaxy images at the diffraction limit with a resolution  $R=2000$  we will map the velocity field across entire galaxies to explore the Tully-Fisher relation at increasing redshifts. This will produce a direct measurement of the distribution of halo masses at each redshift for comparison with the model predictions.

## References

- Baugh C M, Cole S M, Frenk C S, & Lacey C G, 1998, ApJ, 498, 504.
- Dressler A, Oemler A, Couch W J, Smail I, Ellis R S, Barger A, Butcher H R, Poggianti B, & Sharples R M 1997, ApJ 490, 577.
- Lilly S J, Le Fèvre O, Hammer F, & Crampton 1996 ApJ 460, L1.
- Madau P, Ferguson H C, Dickinson M E, Giavalisco M, Steidel C C, & Fruchter A, 1996 MNRAS 283, 1388.

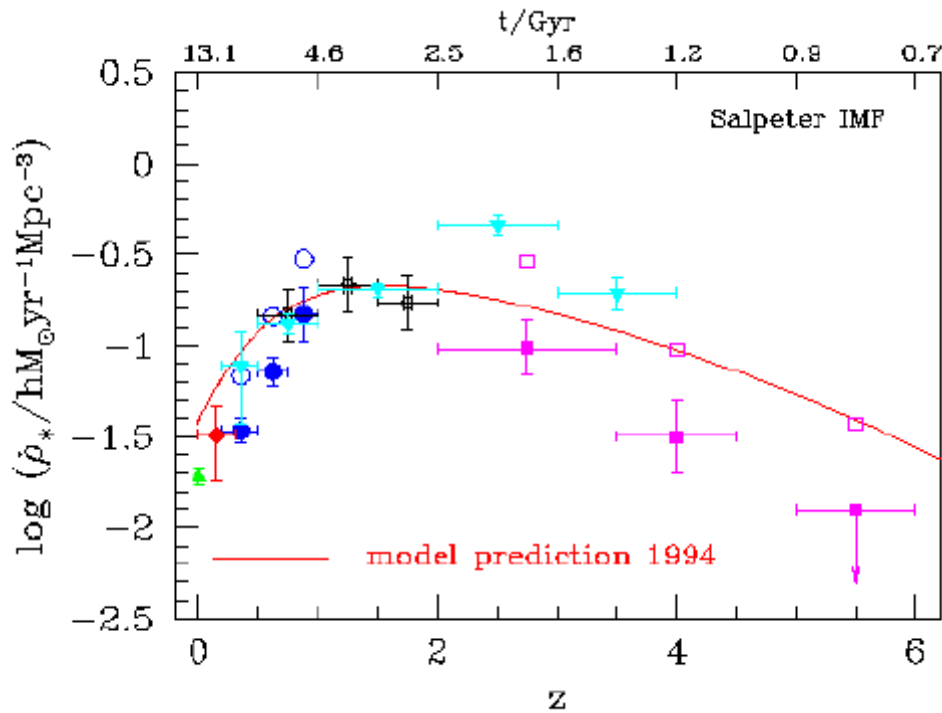


**Figure 1:** The star formation history of the universe (from Baugh et al., 1998, ApJ, 498, 504)

#### 4.2.1.2 Science case no.2: Large scale structures, clustering, (proto-) clusters

Understanding the formation and evolution of large scale structures is a long time quest for cosmology. While we have made significant progress and more is expected with the 8-10m class ground based telescopes, the question of the early formation of the most massive structures will remain a cornerstone of cosmological investigations until a complete picture is drawn.

The comparison of the most recent numerical simulations describing the total mass and the galaxy distributions provide important constraints on theoretical models of cosmic scenarios (see e.g. White, 1996). Our current view is that galaxies, clusters of galaxies and large scale structures grow from primordial density perturbations which subsequently evolve through gravitational interactions (Peebles, 1980, 1993). From the true mass distribution inferred by weak lensing analysis, and from the deep redshift surveys, many outstanding issues can be addressed: the amount of dark matter with respect to the baryonic matter, the mass function of gravitational structures as a function of epoch, constraints on the shape of the power spectrum of initial mass fluctuations to be compared with observation of the microwave background, the physics in place during the non-linear growth of perturbations.

Redshift surveys in our local universe already show that galaxies are located in sheet-like structures, suggesting that the mass could be strongly clustered in filaments, super-clusters and clusters, at the periphery of large voids (da Costa et al., 1998, Landy et al., 1996, Vettolani et al., 1998). Even on the largest redshift surveys in our local universe, covering large angular sizes, there is convincing evidence that the distribution is inhomogeneous on all scales smaller than 100 Mpc. The distribution remains strongly inhomogeneous even out to  $z \sim 1$  (Le Fèvre et al., 1996), with galaxies distributed in an alternance of density peaks and empty regions ("picket-fence" distribution).

At redshifts beyond 1, very little is known about large scale structures. Only a few large structures have been identified so far (Giavalisco et al., 1994, Le Fèvre et al., 1994, Pascarella et al., 1996, Francis et al., 1996, Steidel et al., 1998). Significant clustering of galaxies has been observed at  $z \sim 3$  (Steidel et al., 1998, ApJ, 492, 428), still within the predicted range of models such as the CDM (Governato et al., 1998). At these redshifts, the prevalence of clusters, proto-clusters, or other large scale structures in the distribution of galaxies, is as yet unknown, and the evolution of structures may well be in a critical stage, where observations can directly constrain cosmological models. At  $z \sim 2-3$ , one expects to see the rapid development of non linear clustering in the densest environments such as clusters of galaxies.

In the redshift range 1-3, much progress on our knowledge of large scale structures and their evolution is expected from the large surveys of  $10^5$  galaxies which are planned with the ground-based 8-10m telescopes. At the VLT, the VIRMOS survey will obtain spectra for  $10^5$  galaxies out to  $z \sim 1.2$ ,  $5 \times 10^4$  spectra out to  $z \sim 3-5$ . The sensitivity of these surveys will reveal the large scale structures at  $z \sim 1-3$  only from the bright  $L^*$  galaxies.

It is most probable that the early phases of large scale structures assembly will still remain to be explored after the work from the 8-10m ground based telescopes has leveled down. This is where the NGST is expected to play a unique role.

The NGST will be in a unique position to study:

- . the very early epoch of clusters and other large scale structures formation, beyond  $z \sim 3$ , an epoch for which competing world models show important differences in their predictions
  - . map the distribution of proto-galaxies
  - . compute the evolution of the two-point correlation function
  - . investigate the clustering properties of bright vs. faint, early-type vs. late type galaxies
  - . obtain the mass spectrum of structures from dynamical and lensing properties
- . the detailed kinematics of galaxies and sub-structures forming clusters, filaments, or large scale structures, from sub- $L^*$  to  $L^*$  galaxies

The science requirements from this field are summarized in Table 2.

## References

- da Costa, N., et al., 1998, AJ, in press (July 98, astro-ph/9804064)
- Francis et al., 1996, ApJ, 457, 490
- Giavalisco, et al., 1994, ApJ, 425, L5
- Governato et al., 1998, Nature, 392, 359-361
- Pascarella et al., 1996, ApJ, 456, L21
- Peebles, P.J.E., 1980, "The large scale structure of the universe", Princeton Series in Physics, Princeton University Press
- Peebles, P.J.E., 1993, "Principles of Physical Cosmology", Princeton Series in Physics, Princeton University Press
- Landy et al., 1996, Las Campanas Redshift Survey, ApJ, 456, L1
- Le Fèvre et al., 1994, ApJ, 424, L14
- Le Fèvre et al., 1996, ApJ, 461, 534
- Steidel et al., 1998, ApJ, in press (astro-ph/9708125)
- Vettolani, G., Zucca, E., et al., 1998, A&A.Supp., in press (astro-ph/ 9805195)
- White, S.D.M., proc. ESO Astrophysics Symposium "The early universe with the VLT", Bergeron Ed., Springer, 1996, p.219

### **4.2.1.3 Science case no.3: Evolution of the morphology and dynamics of galaxies**

Unveiling the origins of galaxies is a cornerstone scientific goal of modern cosmology. The Hubble Space Telescope and large telescopes on Earth have for the first time turned the evolution of the general galaxy population at significant redshifts into an observational science. The state-of-the-art data from e.g. the Canada-France Redshift Survey and the Hubble Deep Field strongly suggest:

- . an increase in the proportion of morphologically peculiar systems with redshift
- . the presence of a peak in the cosmic star formation density at redshifts between 1 and 2.

These tantalizing results are the first successes on the way to a full understanding of the dynamical and morphological evolution of galaxies with cosmic time. Still, fundamental questions remain unanswered:

- . when were galaxies assembled, starting from the extremely smooth microwave background revealed by the COBE satellite? Is their star formation history very different from their 'mass aggregation' history?
- . what is the physical origin of the structural variety shown by present-day galaxies, i.e., of the Hubble sequence?
- . what process put in place the observed scaling relations in different galaxy populations?

Spectroscopic capabilities aboard the Next Generation Space Telescope will open up entirely new possibilities for studying the morphological and dynamical evolution of galaxies. The near-infrared wavelength window gives access to crucial diagnostics up to very high redshifts. In the spectral region out to 5 micron, the rest-frame visual light will be sampled out to a redshift of 10, allowing the detection of early-type galaxies at those early epochs, if present. K-corrections in the infrared are much smaller than in the optical region, significantly reducing uncertain steps in the analysis. Key emission lines such as H $\alpha$  and [OII] 3727Å will be available out to redshifts of 6.6 and 12.4 respectively. Rest-frame ultraviolet emission, tracing the youngest stellar population, will be mapped to redshifts greater than 20, while Lyman alpha emission will be available out to a redshift of 40!

IFMOS aboard NGST will play a fundamental role in solving the key questions summarized above by fulfilling the essential requirements for a systematic and unbiased study of galaxy evolution. In particular, NGST-IFMOS will provide, in the crucial 1-5 micron window, integral-field/multi-object capability for (spatially resolved) spectra of a large number of objects to considerably faint flux limits, thereby allowing one to establish:

1. The evolution of morphologies. This requires redshift determinations for more than a thousand galaxies, preselected to form a statistically complete sample covering different morphological types as well as apparent magnitudes and colours
2. The formation of disks. Our current understanding of the morphological evolution of galaxies suggests that disks are a relatively recent acquisition, having formed mostly at redshifts smaller than 2. A strong evolution in the sizes of star-forming disks between  $z=2$  and  $z=0$  is predicted, low- $z$  disks being on average much larger than high- $z$  disks. An efficient integral-field spectrograph in the near-infrared will provide a detailed map of the redshifted H $\alpha$  emission from a suitable sample of disks in the relevant redshift range. This will not only yield the evolution of disk sizes with redshift, but also reveal the star formation patterns in the disks, and thus the detailed mechanism of disk assembly.
3. The interaction and merger rates. Interaction and merger events dramatically change the structural properties of galaxies, and trigger bursts of star formation that significantly affect the properties of the stellar population of the merger product. Therefore, understanding the evolution of interaction and merger rates as a function of environment is integral to understanding the entire process of galaxy formation and evolution, the morphology-density relation, and the origin of the Hubble sequence. The velocity scale at which interactions occur is an important parameter; mergers can occur with velocities of the order of the internal velocities of galaxies. A spectral resolution of at least  $\sim 3000$  is necessary to separate interacting galaxies from fly-bys and projections.

4. The cosmic star formation history. Current derivations of the cosmic star formation history are based on rest-frame ultraviolet measurements: the unknown effects of extinction represent the single greatest uncertainty in these results. A survey of H. emission in a magnitude-selected sample of 1000-10000 galaxies out to very high redshifts will greatly alleviate these difficulties: it will provide not only a direct measurement of the cosmic star formation history, but also of the evolution of the luminosity function of the star-forming galaxies.
5. The dynamical evolution of galaxies. Rotation velocities and velocity dispersions for samples of more than a thousand early-type and late-type galaxies, as a function of redshift, will reveal the dynamical evolution of these populations, as well as the evolution of the Tully-Fisher relation and of the fundamental plane of early-type galaxies. In hierarchical scenarios, galaxies build up from smaller fragments of low masses and thus low circular velocities; current data suggest the need to be able to resolve line widths as low at 70 km/s or even less. This requires a spectral resolution of at least 5000, i.e., a significant technological challenge, and one of the important performance parameters to be assessed in unison with other trade-offs.

Clearly, these projects are interrelated, and our final understanding of how the morphological and dynamical properties of the present-day universe have come to be will eventually depend on matching together the different answers in a consistent picture. In our study we have made a detailed trade-off analyses with all these particular objectives in mind, in order to arrive at the best instrument design for taking on the challenging task of unravelling the morphological and dynamical evolution history of galaxies in the Universe.

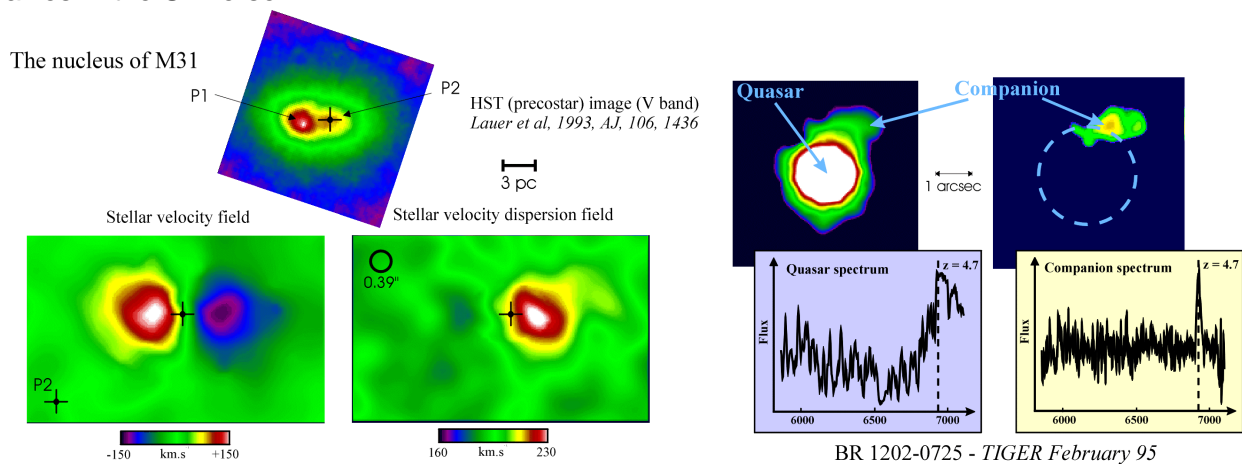


**Figure 2:** Integral Field Spectroscopy of (left) the core of M31, (right) a QSO and companion at  $z=4.7$  (CFHT and Tiger)

#### 4.2.1.4 Science case no.4: Strong and weak lensing

Gravitational lensing has emerged as one of the most important new tools of the modern cosmologist. Significant progress has been made with ground-based telescopes and HST in constraining mass distributions on various scales and in exploring the nature of faint magnified systems that would otherwise be too faint for detailed study (see recent reviews by Narayan & Bartelmann 1996, Mellier et al 1996). The phenomenon can also be used to great advantage in surveying for distant sources at a variety of wavelengths (c.f. Smail et al 1997).

Long-slit and multi-object spectroscopy has played a crucial role in constraining the lensing geometry, particularly in clusters where lensed sources can be recognised with moderately good image quality via their distorted appearance (c.f. Kneib et al 1996). Spectroscopic data of moderate resolution yields

redshifts and star formation characteristics for individual sources (Ebbels et al 1996) and a complete mapping of the lens is possible in restricted cases (Ebbels et al 1998).

In exploring the near/mid IR wavelength range accessible to NGST, more distant and physically smaller sources are likely to be found and it is possible that even exquisite imaging data will be unhelpful in isolating those which are lensed. An interesting possibility offered by integral field spectroscopy with the NGST is the complete spectral mapping of the cores of distant clusters for lensed sources whose magnifications would typically be 2-5. The Einstein radius for the most distant massive clusters available when used to probe sources of redshift 5-10 is  $\sim 10$  arcsec depending on the cosmological model. A high angular resolution IFU survey sensitive to emission lines sources in the 1-5 micron range would extend the coverage of weak H alpha emission to  $z=6.5$  as well as probing the presence of more distant sources with other diagnostic lines. Any population with a steep source count will be very effectively probed via such techniques.

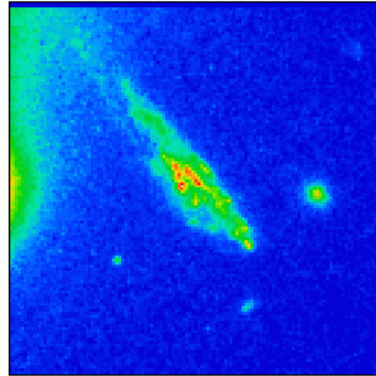
The high angular resolution of an IFU on NGST-IFMOS will also be effective in known cases of strong lensing where the additional angular magnification can be used to great effect. Such work has begun for extended sources at  $z=1$  by using HST imaging in conjunction with ground-based IFU spectroscopy (Figure 3). At the moment only the most luminous sources can be studied because of the large surface brightness losses. Furthermore, reliable diagnostics of star formation less affected by dust extinction can only be probed in the near-IR where the background is high. The huge gain in sensitivity for background-limited spectroscopy in the near/mid IR with NGST will enable the detailed mapping of numerous  $z>2$  lensed sources found from systematic imaging of dense cluster cores.

On the smallest angular scales, the remarkable angular resolution of NGST might permit direct studies of galaxy-galaxy lensing using fine sampled IFU data. Thus far, galaxy-galaxy lensing has only been examined statistically by correlating galaxy properties in pairs with projected HST data (Ebbels 1998). However, given a sufficiently high surface density of sources, the rate of strong lensing expected due to galaxy halos is sufficient ( $\sim 0.2$ - $0.5\%$  depending on physical properties) to yield an adequate number within a 1-2 arcmin field. 3-10 are expected in the HDF alone (Hogg et al 1996). The absolute surface density depends on the redshift distributions of the source and deflector populations which, when measured directly, may probe the cosmic geometry and the lens properties as a function of redshift. The systematic exploitation of this phenomenon has hardly begun and is well suited to pixel-by-pixel spectroscopy where coincidences are expected in redshifts over a 5 arcsec field (Figure 4).

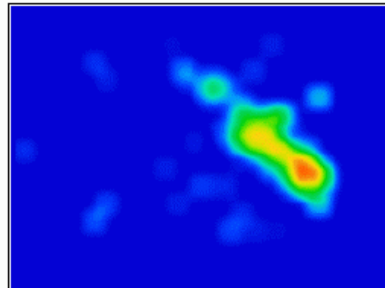
## references

- Ebbels, T. 1998 Ph.D. thesis, University of Cambridge
- Ebbels, T., LeBorgne, J-F, Pello, R., Ellis, R.S., Kneib, J-P, Smail, I. & Sanahuja, B. 1996 MNRAS 281, 75.
- Ebbels, T., Ellis, R.S., Kneib, J-P., Le Borgne, J-F, Pello, R., Smail, I & Sanahuja, B. 1998 MNRAS 295, 75.
- Hogg, D., Blandford, R., Kundic, T., Fassnacht, C.D., Malhotra, S., 1996 Ap J 467, L73
- Kneib, J-P, Ellis, R.S., Smail, I., Couch, W.J. & Sharples, R.M., 1996 Ap J 471, 643.
- Mellier, Y., van Waerbeke, L., Bernadeau, F. & Fort, B. in 'Neutrinos, Dark Matter & the Universe' 1996 (astro-ph/9609197).
- Narayan, R. & Bartelmann, M. 1996 (astro-ph/9606001)
- Smail, I., Ivison, R. & Blain, A.W. 1997 Ap J Lett 490, L5.
- Soucaill, G., Kneib, J-P, Picat, J-P & Ellis, R.S. 1997 in the Young Universe, ed. D'Odorico, S. et al, ASP Conference Series, in press.

HST F702W  
image



Reconstructed image of the arc  
in the 3727Å emission line



Velocity field

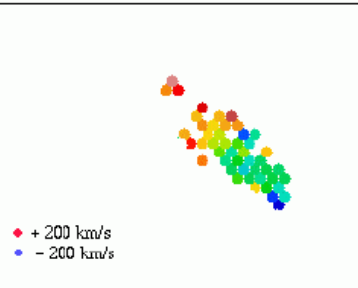


Figure 3: The dynamical study of a lensed galaxy with  $z=1.018$  from Argus spectroscopy (Soucail et al 1999)

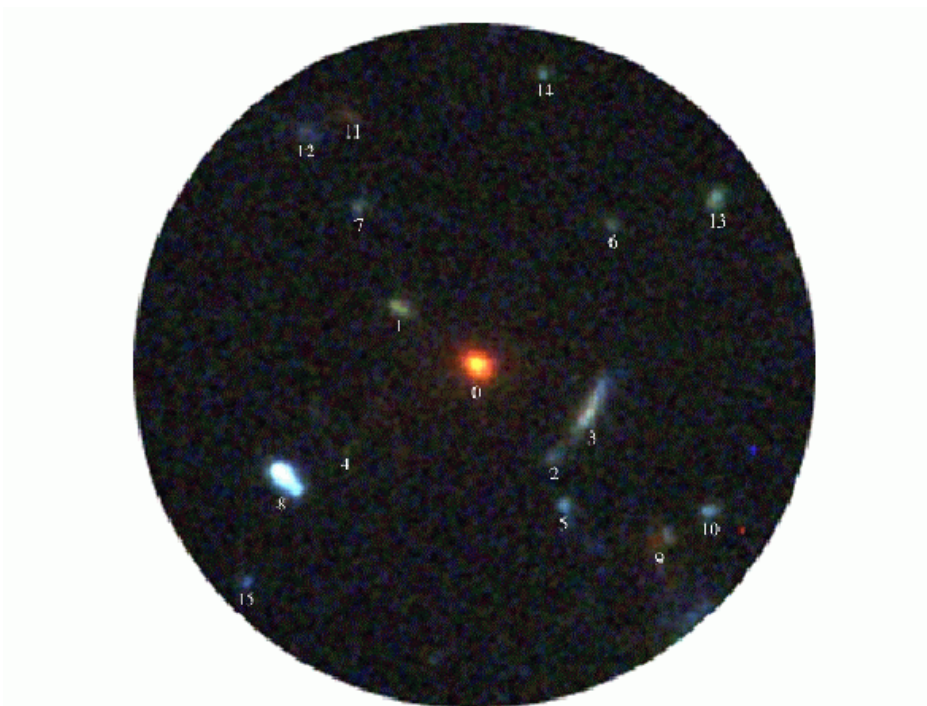


Figure 4: A possible example of galaxy-galaxy lensing in the HDF following Hogg et al (1996). The 16 possible components of a distant image lie within a 5 arcsec field. The spectroscopic study of more distant and fainter examples is ideally suited to a IFU.

## 4.2.2 Science requirements

From the discussions of science cases above, and in line with the NGST-DRM, we have derived the science specifications presented in Table 2.

**Table 2:** science requirements

Science Area Science case no.	range	N <sub>objects</sub>	Simultaneous max / min	Field	Sampling	Spatial elements	R spectral
Evolution of Galaxies 1	(0.6) 1-5	10 <sup>6</sup>	2-3	As large as possible (10')	0.3"	4x10 <sup>6</sup> max	200-3000
Large Scale Structures 2	1-5	5x10 <sup>6</sup>	2	As large as possible (10')	0.3"	4x10 <sup>6</sup> max	200-3000
Galaxies Dynamics: 3	1-5	10 <sup>3</sup> -10 <sup>4</sup>	½	<3"x3"	0.01-0.04"	10 <sup>5</sup>	5000
Chemical Evolution	1-5	10 <sup>3</sup> -10 <sup>4</sup>	2	<3"x3"	0.3"	<4x10 <sup>6</sup>	3000
Stellar Populations	1-5	10 <sup>3</sup> -10 <sup>4</sup>	2	<3"x3"	0.01-0.04"	10 <sup>5</sup>	3000
Weak and Strong Lensing: 4	1-5	10 <sup>3</sup> -10 <sup>4</sup>	2	<5"x5"	0.01-0.04"	2.5x10 <sup>5</sup>	200-3000

## 4.3 REQUIRED OPERATING MODES

The operating modes are identified as follows:

- . Wide Field low resolution 2D spectroscopy
- . Narrow Field high resolution 2D spectroscopy
- . Calibrations
- . Data Processing

We assume that the pointing/tracking, and data transfer operations are handled by the spacecraft.

## 4.4 INTEGRAL FIELD SPECTROSCOPY VS. MULTI-SLIT SPECTROSCOPY

The issue of the complementary needs for an integral field spectrograph vs. a multi-slit spectrograph is approached here from a purely astronomical point of view. We give below several key elements which motivate the IFS or the MOS approach. Our conclusion is **that to address the key NGST science goals, an IFS is required**. See section 10 for more details.

#### 4.4.1 Arguments in favor of an IFS

We give below some examples of programs for which the IFS approach is most efficient. This shows how versatile this concept is.

*Deep galaxy surveys:* the identification of very distant galaxies critically depends on the selection criteria applied to isolate a galaxy population. The great advantage of an IFS approach for deep galaxy surveys is that there is no need for a priori selection from imaging data. When set on a given pointing, an IFS will provide spectra of ALL objects in the field. The IFS does not impose any particular geometry on object sampling, and allows to optimally extract spectra over the full object extension, not restricted to a slit of fixed width like slit spectrographs, therefore eliminating the slit loss problem. An IFS is thus particularly sensitive to the faint slightly extended objects seen at the limiting sensitivity of the HST Hubble deep fields.

At the faint sensitivity limits of NGST, an IFS with a field  $\sim 45 \times 45$  arcsec<sup>2</sup> is equivalent to a multi-slit spectrograph with a field  $3 \times 3$  arcmin<sup>2</sup>, in terms of speed of acquisition of a similar size sample.

*Spectroscopy of mergers at early epochs:* With the impressive sensitivity and spatial resolution provided by the NGST, it will be possible to perform spatially resolved spectroscopy of galaxies at  $z \gg 1$ . The kinematics and dynamics of the building blocks of present day galaxies can be probed with an IFS. If hierarchical structure formation models are correct, galaxy mergers are very common in the early history of the universe. Slit spectra fail to resolve the two or more galaxies involved in a merger/interaction, providing potentially erroneous results by combining the spectra of the two components.

*Spectroscopy of extended objects:* Evidence from the Hubble Deep Field imaging shows that a large number of galaxies are spatially resolved at the resolution of the HST. At NGST sensitivities and resolutions, an ever larger fraction of objects will be spatially resolved (see Section 10). Galaxy rotation curves, kinematics of narrow line regions in active galaxies, age and metallicity determination of star forming regions, demographics of black holes in galaxy nuclei can all be investigated with spatially resolved spectra at the telescope diffraction limit.

*Spectroscopy in crowded fields:* Multi-slit spectrometers are ill-suited to work in crowded fields, such as the cores of galaxy clusters, globular/open star clusters, lensed galaxy images near foreground cluster cores, environments of QSOs etc. due to a limit on the maximum density of spectra before they overlap. At the depths reached by the NGST, most fields will suffer substantially from foreground confusion and crowding effects, making it difficult to obtain uncontaminated spectra of distant background objects. An IFS does not face these problems.

*Quasar Host Galaxies:* Relatively little is known about QSO hosts, because they are very faint objects in the near vicinity of a very bright point source. Two dimensional information about the Point Spread Function (PSF), as can be obtained with an IFS, can be effectively used to subtract the light of the QSO very accurately, and thus obtain a spectrum of the faint host galaxy. A gain of two magnitudes in sensitivity is easily achievable with this technique.

## 5 CONCEPT REVIEW – TRADE-OFF ANALYSIS

### 5.1 REVIEW OF POSSIBLE CONCEPTS

The main integral field spectroscopy concepts are as follows:

- . Fibers only
- . Lenslets only
- . Fibers coupled to lenslets
- . Image Slicer

Additional concepts are:

- . Fourier Transform Spectrometer
- . Fabry-Perot Spectrometer

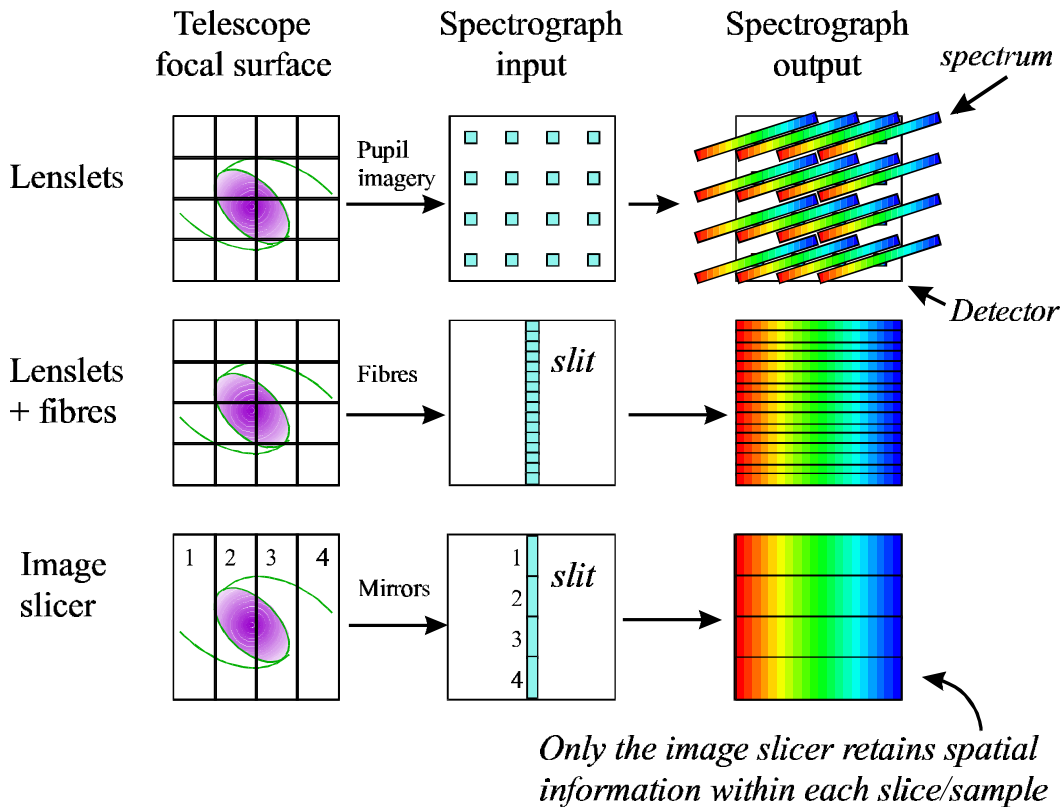


Figure 5 : Integral field spectroscopy possible concepts

## 5.2 SUITABILITY ASSESSMENT

Table 3 : Concept suitability assessment

Concept	Field	Spatial Sampling	Simultaneous wavelength	Complexity	Technology risk
Lenslet only	-	+	+	++	++
Fibers only	-	-	++	++	+
Fibers+lenslets	+	++	++	+	+
Image Slicer	+	++	++	+	+
Fourier Transform Spectrometer	++	+	-	-	+
Fabry-Perot Spectrometer	++	+	-	-	+

The following designs are potentially suitable for NGST:

- . The **Fibers+lenslets** concept
- . The **Image slicer** concept
- . The **Fourier Transform Spectrometer** concept
- . The **lenslet** only concept

The fibers+lenslets concept and the image slicer concept are the most suitable to the NGST context as presented in Table 3. However, the fibers+lenslets concept relies on fiber optics technology which is not yet space qualified, and this concept offers a lower spectra packing capability than the image slicer concept because fibers have to be spaced to minimise cross talk.

**We have therefore selected the image slicer concept as the baseline** for the detailed instrument study.

### 5.3 TECHNICAL SPECIFICATIONS

The technical specifications defined at the mid-term review of the study are presented in Table 4.

**Table 4 : IFMOS Technical Specifications**

Item	Specification
Input F/	24
Wavelength range	1-5 .m
Field of View, low spatial resolution	~1'x1'
Spatial sampling, low resolution	0.3 arcsec / pixel
Field of View, high spatial resolution	~6"x6"
Spatial sampling, high resolution	0.03 arcsec / pixel
Spectral resolution	200 to 2000 essential up to 5000 desirable
Throughput optical train	>70%
Number of detector pixels	Baseline 8192x8192 pixels
Building block array	2048x2048 pixels
Pixel size	18.5 .m
Detector RON	5 e-/read
Detector QE	80%
Detector dark current	0.02 e-/s
Detector full well	100000 e-
Detector read-out time	10 <sup>-6</sup> s/pix
Spectrograph operating Temperature	30-50K

## 6 DESIGN OVERVIEW

### 6.1 INSTRUMENT DESIGN

Based on the technical specifications given in Table 4, we have designed the instrument around two channels, which can work in parallel.

Low resolution, wide field channel (Figure 6)

This channel maximizes field coverage and sensitivity for an integral field spectrograph. It works in a regime where sensitivity is limited by background. The field is  $40 \times 46$  arcsec<sup>2</sup>, which allows to take spectra of several hundred galaxies simultaneously at the depth of the NGST. With spatially resolved elements of 0.2 arcsec on the sky, it is well suited to get spectra of objects with equivalent radius on order 0.1 arcsec, detected at the faintest limit of the NGST at  $R \sim 150$ .

High resolution channel (Figure 7)

This channel is designed to take spectra of single objects, or objects in a compact group. The 3D approach allows to get spectra for all resolved elements each 0.05 arcsec in a field  $3.8 \times 2.6$  arcsec<sup>2</sup> at a spectral resolution  $R \sim 3000$ .

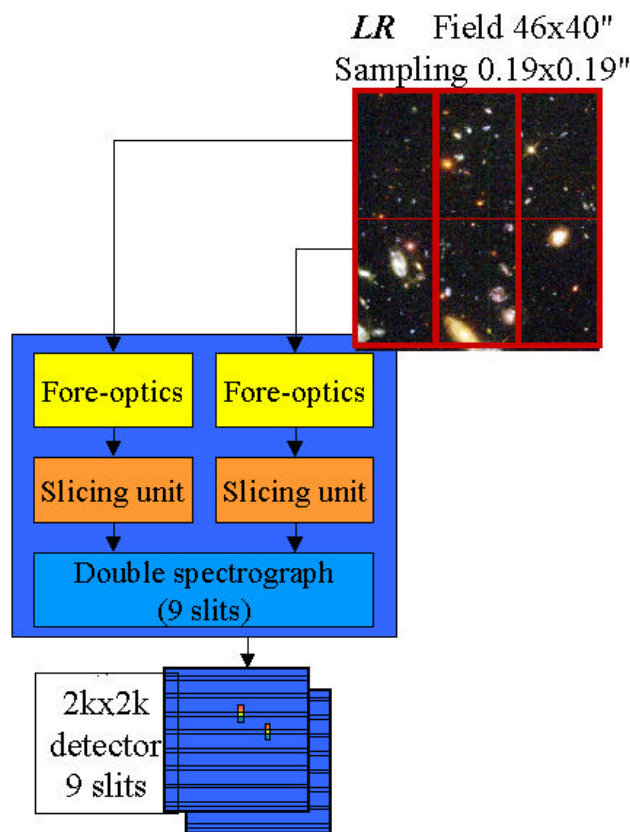


**Figure 6** : Low resolution channel concept

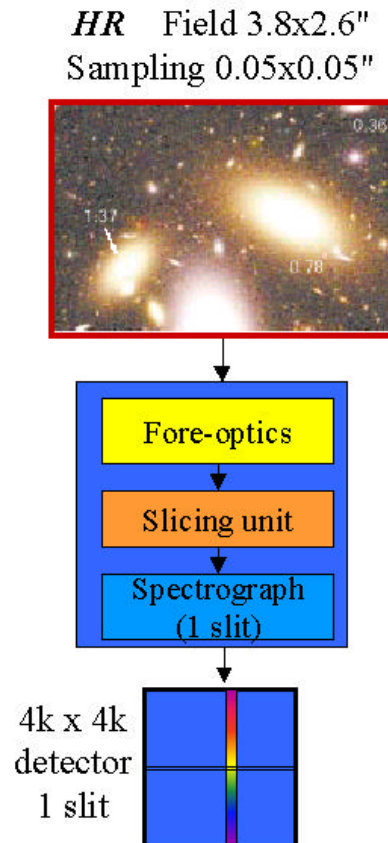


**Figure 7** : high resolution channel concept

## 6.2 DESIGN TRADES

The selected design results from the relative allocation of detector pixels to spatial and spectral pixels. We have allocated 6x2kx2k pixels to the low resolution channel and 4x2kx2k pixels to the high resolution channel. This obviously could be different if relative weight of science requirements are adjusted.

The detectors are the main limiting factor: array size, read noise and dark current are setting the overall performances. We have adopted the same detector parameters as the requirements set by the NGST project office for detectors development: 0.02 e<sup>-</sup>/pix/s dark current and less than 5 e<sup>-</sup> read noise.

### 6.2.1 Low resolution channel

The main design parameters are:

1. The spatial resolution elements 0.19x0.19 arcsec<sup>2</sup> are defined to match the size of the faintest galaxies seen today by HST.
2. The spectral resolution R~150 is set to provide the best compromise between sensitivity and velocity measurement at better than 100km/s
3. The full wavelength range 1.25 to 5 microns is covered in one shot
4. With 6x2kx2k pixels, the above spatial and spectral sampling, the maximum field is 40x46 arcsec<sup>2</sup>.

The choice on points 1 and 2 is limited by the requirement to work in the background limited, photon noise regime. For spatially resolved elements of 0.19x0.19 arcsec<sup>2</sup>, the maximum spectral resolution is set to R~300, using the current detector dark current and read noise goals. At R~300, spectra are twice as long as at R~150, using this resolution would cut the field by half.

One could work at R~300 in the same field, by relaxing the requirement to have a full wavelength coverage: two exposures would be required to get the full wavelength coverage (which might not be required for all programs).

### 6.2.2 High resolution channel

The main challenge here is to maximize the field while keeping the high spatial and spectral resolution. Spatial resolution elements of 0.05x0.05 arcsec are a compromise to increase the background to minimize the severe constraint of being limited by the detector read noise and dark current.

A spectral resolution R~3000 has been set as a requirement. This requires a significant allocation of detector pixels to spectral rather than spatial elements. Relaxing this constraint to R~1500 would either allow a field twice as big, a spatial sampling twice finer, or a full wavelength coverage 1.25 to 5 microns by adding a dichroic and a camera.

We have only one spectral resolution in this mode to allow for a simple grating mechanism. A more complex mechanism would allow more gratings hence more resolution choices.

## 7 OPTICAL DESIGN DESCRIPTION

### 7.1 DESIGN DRIVERS

The drivers for the design definition were:

- . Assume that 2Kx2K, 18 microns pixels detectors will be available
- . Spatial sampling in HR mode: adequate sampling of the diffraction pattern, while working as close as possible to the photon noise regime (0.05 arcsecond sampling preferred to 0.03)
- . Spectral resolution in HR mode: R=3000 is a science requirement and allows to fill 2 detectors with the complete spectrum of one octave
- . For the LR channel, the instrument field x sampling x spectral resolution x spectral coverage was constrained by the overall weight of the instrument, set to a maximum of 150kg by ESA for the purpose of this study
- . In the LR channel: one camera per detector, and one collimator for two cameras, has been identified to maximize performances.
- . The wavelength coverage in the LR mode is set to 1-5 microns simultaneously
- . In order to optimize the sampling versus the field, 1 resolution element on the sky is projected on 2 x 1 pixels on the detector (1 element for spatial resolution and 2 for spectral resolution)
- . To relax constraints on the slicer manufacturing, we have to magnify the field before slicing
- . To limit the losses by diffraction, we have to oversize the spectrographs (we limit the maximal speed of the cameras at 2.5, for manufacturing, tolerancing & integration purpose)

Table 5 gives a summary of the design performance

**Table 5** : Design performance summary

Number of detectors	10 (2k x 2k)
Wavelength Coverage	1.25 – 2.5 and 2.5 – 5 $\mu\text{m}$ (2 octaves)
High Resolution channel, spectral resolution R	3000 @ 1875nm
High Resolution channel, spatial sampling	0.05"
High Resolution channel, field of view	3.8 x 2.6"
High Resolution channel, throughput	0.5 – 0.6
Low Resolution channel, spectral resolution R	~150
Low Resolution channel, spatial sampling	0.19"
Low Resolution channel, field of view	46 x 40"
Low Resolution channel, throughput	0.5 – 0.6

## 7.2 MAIN SUBSYSTEMS

Each of the instrument channels is made of the following subsystems (from the telescope):

1. **Pick-up unit** to sample the field from the telescope focal plane
2. **Magnification and scaling adaptation**
3. **Image slicer** and formatting into long slits at spectrograph entrance
4. **Spectrograph** with a collimator, dispersive element, camera and detector

The high resolution channel uses a **double pass spectrograph**.

To keep the optics simple, the wide field channel is separated in 3 small spectrographs with small optical elements.

## 7.2.1 Pick –up mirror and field of view:

The field of view of the instrument is  $40 \times 46$  arcsec<sup>2</sup> (LR) and  $3.8 \times 2.6$  arcsec<sup>2</sup> (HR). The smaller field is positioned on one side of the large field. One very important point is that the two mode are working in parallel. The LR field is cut in 6 parts, feeding 6 fore optics modules.

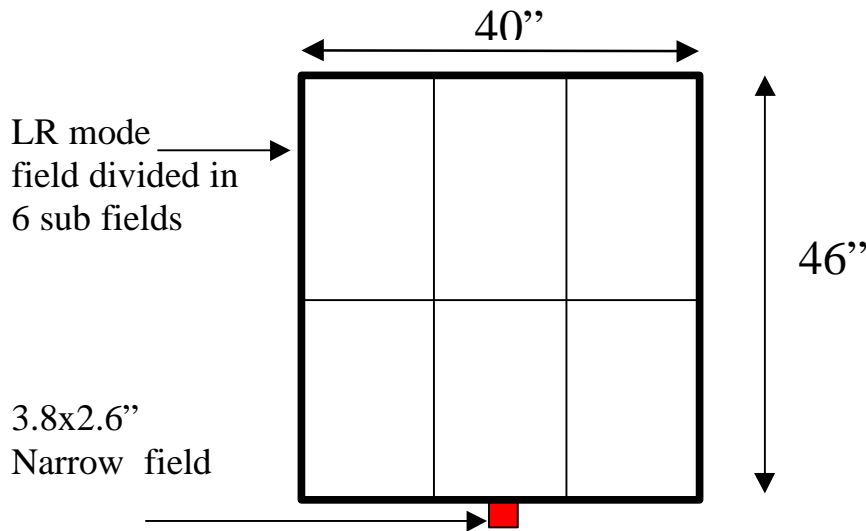


Figure 8: IFMOS Field of View

## 7.2.2 Fore optics

To feed the spectrograph, we need to have different magnifications along the slit and in the dispersion direction. This is done by the fore optics.

To optimise the performances of the slicer, a convenient solution is to have 6 *fore-optics units* feeding one mirror slicer each.

Each LR fore optics unit has the following properties:

- F/24 scaled into **F/120x F/60**
- Magnification : **5.06** in the dispersion direction and **2.51** in the slit direction
- F.O.V.: ~ **23.2 x 13.3**.

There is only one fore-optics unit for the HR mode and his characteristics are:

- F/24 scaled into **F/412x F/206**
- Magnification: **17.2** in the dispersion direction, **8.6** in the slit direction

## 7.2.3 Slicing unit

This unit is made of two main elements:

1. Mirror slicer : slice the field in small slits
2. Slit unit: rearrange the small slit in long slits

See section 8.1 for more details.

## 7.2.4 Spectrographs

See section 9 for more details.

## 7.2.4.1 LR spectrograph:

Multiple small spectrographs allow for relaxed tolerancing and more straightforward manufacture. The spectrograph covers two wavelength octaves, 1.25-2.5 microns and 2.5-5 microns simultaneously, with one detector per wavelength channel.

We have selected prisms as the dispersive elements. This choice allows to have high efficiency and no order contamination/overlap from one slit layer to the next.

There is one collimator, and two cameras (3 mirrors each). A dichroic splits the beam into the two octaves feeding the two cameras.

## 7.2.4.2 HR spectrograph

The baseline design is a double pass spectrograph. The advantages of such kind of system are: size, weight.

The system is a three mirror anastigmatic. The dispersive elements are grating with 50-100 grooves per millimetres. The system allows to observe one octave at a time. A grating exchange mechanism allows to select the optimum grating for each octave.

## 7.3 OVERALL IMPLEMENTATION:

The overall implementation is presented in Figure 9.

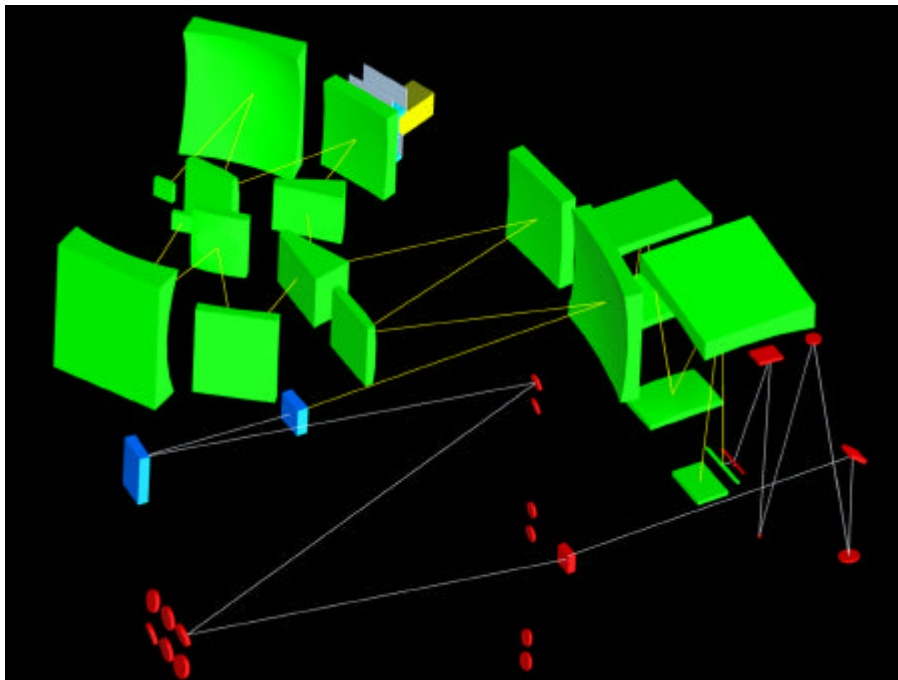


**Figure 9** : overall optical layout , Low resolution channel is on the left (one of 3 modules shown), the High resolution channel is on the right

## 8 IMAGE SLICER OPTICAL DESIGN

This description covers the optical system from the telescope focus to the spectrograph slit. The optical system is divided into two functional units: (a) the fore-optics from the pickoff to the slicing mirror and (b) the slicing unit from the slicing mirror to the slit.

The main features of the designs for the two modes (LR and HR) are summarised in Table 6 and Table 7.

**Table 6 : HR mode summary**

Field	3.8 x 2.6 arcsec
Sampling	0.05 x 0.05 arcsec (projects to 1x2 pixels)
Field pickoff	Direct (no mirror in field)
Subfield division	52 slices of 3.75 x 0.05 arcsec
Number of spectrographs	1
Detector format/spectrograph	4kx4k overall optical layout , HR fore-optics
Number of slits/spectrograph	1
Slit length	205 arcsec (4096 pixels with 4 pixels free between slice images)
Fore-optics components:	3 reimaging + 1 fold mirror
Slicer unit components:	1 x (slicing mirror + pupil mirror + slit mirror) for each slice

**Table 7 : LR mode summary**

Field	46x40 arcsec
Sampling	0.19 x 0.19 arcsec (projects to 1x2 pixels)
Field pickoff	By pickoff mirrors into 6 sub-fields in a 2x3 mosaic
Subfield division	72 slices of 23 x 0.186 arcsec
Number of spectrographs	3 (2 subfields/spectrograph)
Detector format/spectrograph	2kx2k
Number of slits/spectrograph	9
Slit length	380 arcsec (2048 pixels) including 3 free pixels between slice images
Fore-optics components:	1 pickoff + 2 reimaging mirrors
Slicer unit components:	1 x (slicing mirror + pupil mirror + slit mirror) for each slice

### 8.1 OPTICAL PRINCIPLE

#### 8.1.1 Advanced Image Slicer

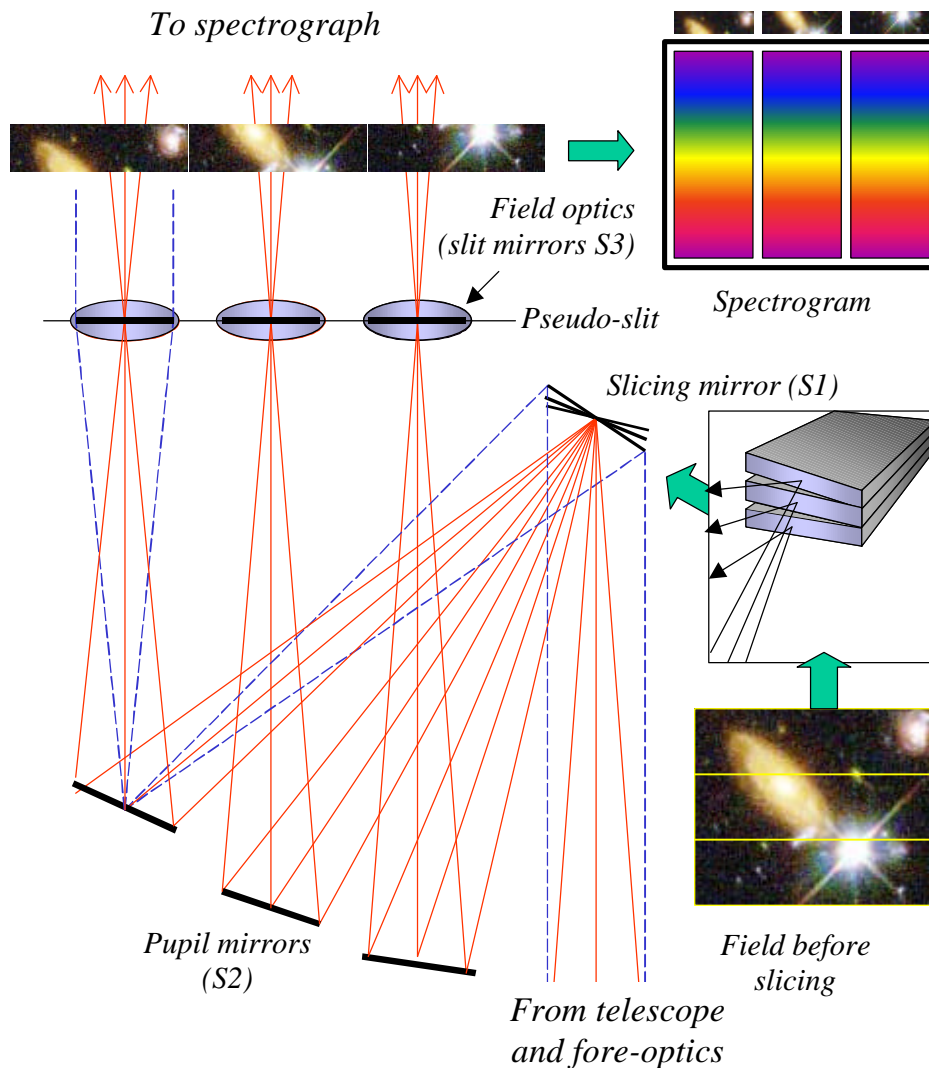


**Figure 10** : Principle of Advanced Image Slicer

The principle of the Advanced Image Slicer (AIS) is illustrated in Figure 10. See Content (1997) for a complete description. The field is imaged onto a slicing mirror which divides the field into a number of slices which are rearranged end-to-end to form the entrance slit of the spectrograph. The AIS concept is derived from that of 3D (MPE; Krabbe et al. 1997). The main difference from 3D is that the optics are curved instead of flat. This brings many benefits since the telescope pupil can be relayed onto the imaging mirrors to reduce their size and reduce off-axis aberrations. The imaging mirrors are also curved to allow the slicing mirror to be imaged onto the slit. Finally, field optics may be placed at the slit to relay the telescope pupil accurately onto the spectrograph pupil.

Image slicing systems makes optimum use of detector surface with minimal dead space and provides continuous mapping of each slice onto the detector. The optics may be diamond-turned from the same material as the mount to facilitate use in cold environments. The sampling element on the sky is square but projects onto 1x2 pixels to permit critical sampling of the slice width in dispersion without compromising the spatial sampling on the sky. This is accomplished via anamorphic magnification in the fore-optics.

A further beneficial feature of image slicers is that diffraction losses only affect the dispersion direction unlike techniques where the field is sub-divided in two dimensions (e.g. fibres and lenslets) which suffer diffraction losses in both directions.

## 8.2 DESIGN ISSUES

Using current design tools, the design must be split into three semi-independent units to correctly simulate broadening of the beam by diffraction:

- . **Fore-optics** (from pickoff to slicing mirror)
- . **Slicing unit** (from slicing mirror to slit)
- . Spectrograph (covered in section 9)

Other parts of optical system not in the unit under study are simulated by paraxial optics (including the telescope).

The quality of the design could be assessed via the following metrics.

- . Comparison with the diffraction limit: *but this is difficult to use since it is wavelength-dependent and ignores the effect of pixel sampling*
- . Geometric spot size: *this is simpler to use but can lead to overdesign in the sense that the effect of diffraction may impose a limit on performance which would allow a relaxation in the optical specification.*

Therefore we have assessed the quality of the design in terms of the *fraction of the field over which 80% geometric enclosed energy is obtained within 1 pixel width. Note that the geometric encircled energy is an upper limit since we assume uniform filling of the diffraction-enlarged pupil.*

It is anticipated that a more detailed figure of merit will be developed for the final design, which will take diffraction into account more fully. This may allow the design to be relaxed.

In the detailed description that follows, the spot diagrams are independent of wavelength since achromatic optics are employed.

## 8.3 DETAILED OPTICAL DESCRIPTION

### 8.3.1 HR fore-optics

The layout is shown in Figure 11 and the spot diagrams on the slicing mirror (S1) in Figure 12.

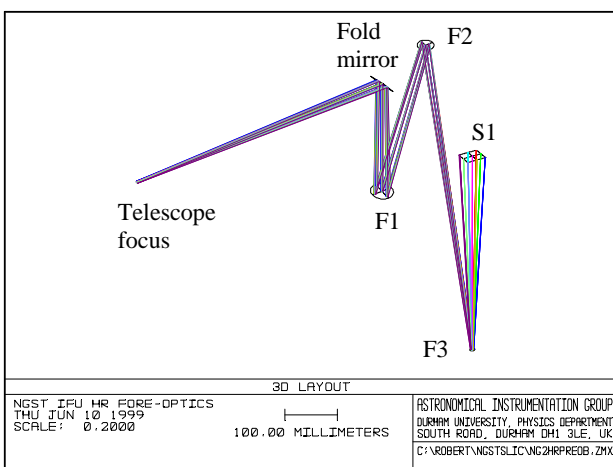


**Figure 11:** HR fore-optics layout. The three mirrors of the fore-optics are labeled F1, F2 and F3. The slicing mirror is indicated by S1.

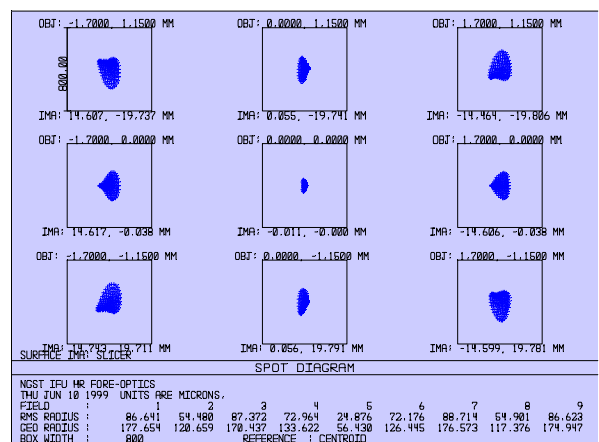


**Figure 12 :** HR mode spot diagrams at S1 over the full field. The box size is the width of the slice

### 8.3.2 HR slicing unit

The layout is shown in Figure 13 where rays are shown for two slices within the slicing mirror. Spot diagrams are shown in Figure 14.

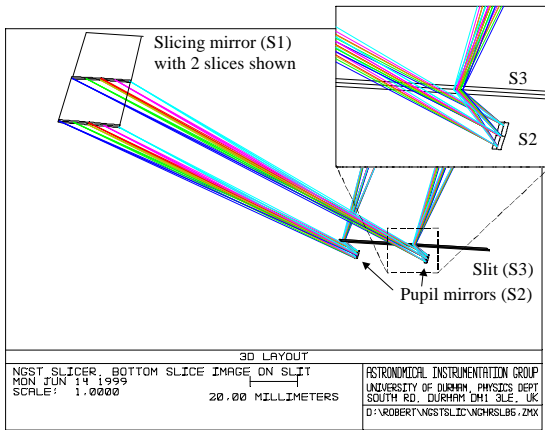


**Figure 13:** HR slicing unit. Rays from two slices are shown

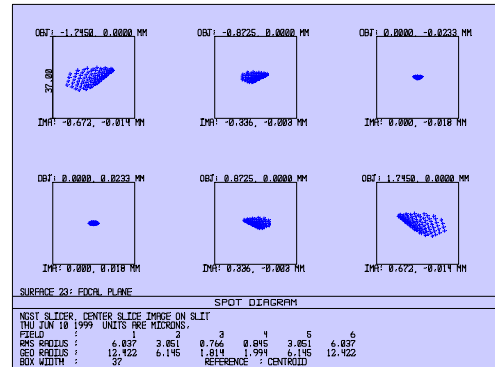


**Figure 14:** HR mode spot diagrams at S3 (the slit) for the central slice for different positions along the slice. The box size is equivalent to 2 pixels on the detector

### 8.3.3 LR fore-optics

The layout of the 6 subfields is shown in Figure 15. Spot diagrams on the central slicing mirror are shown in Figure 16. Spot diagrams for the other three subfields are identical to these.

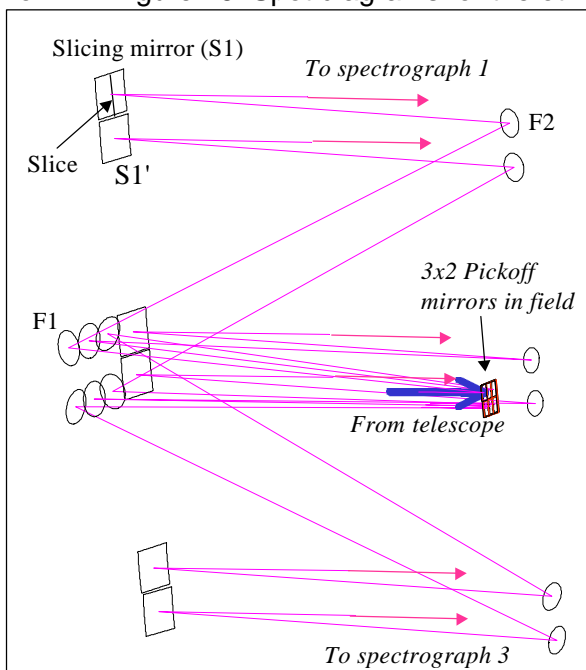


**Figure 15:** LR fore-optics (fore-optics mirrors = F1, F2; slicing mirror S1). S1' indicates the second of each pair of slicing mirrors feeding a single spectrograph.

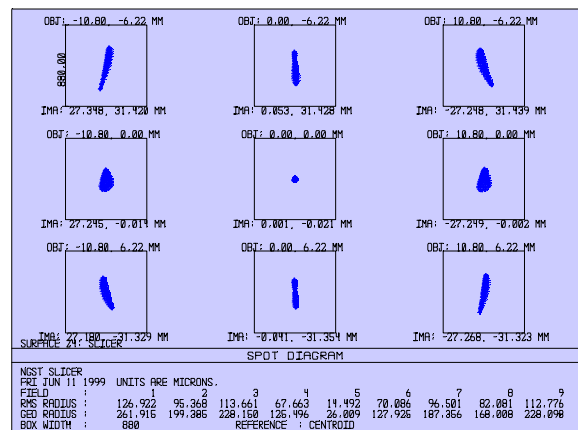


**Figure 16:** LR mode spot diagrams at S1 over the full extent of the central subfield. The box size is equal to the width of a slice

## 8.3.4 LR slicing unit

The layout is shown in Figure 17 for two slices. The spot diagram for one slice (representative of all slices) is shown in Figure 18.

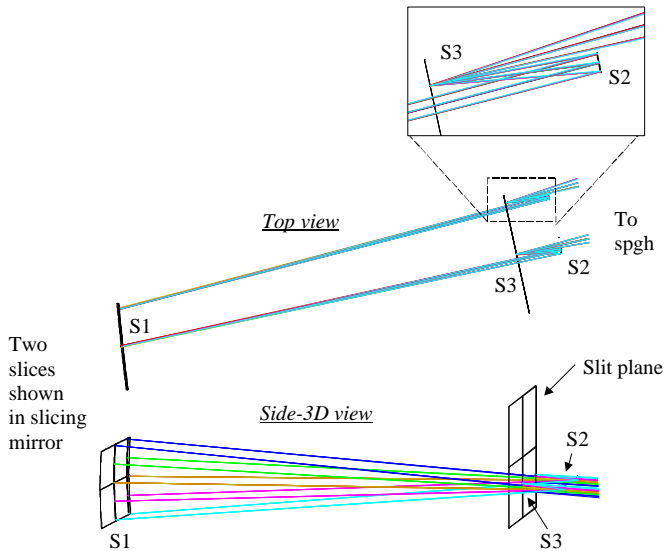


**Figure 17:** Layout of LR slicing unit. Paths from two slices at the slicing mirror (S1) are shown. S2 and S3 are the pupil and slit mirrors respectively.

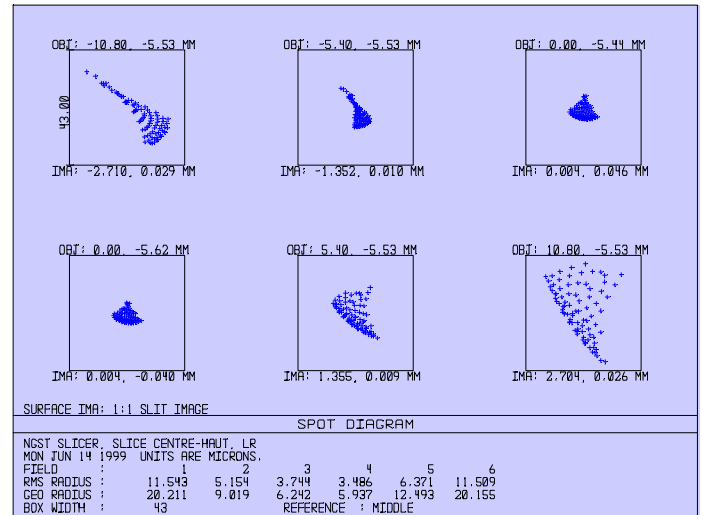


**Figure 18:** LR mode spot diagrams for one slice at S3 (the slit) over the length of the slice. The results for all the slices is very similar. The box size is 1 pixel.

## 8.4 SUMMARY OF SLICER OPTICAL DESIGN

Our analysis of the optical design can be summarised as follows.

- **HR slicer unit** gives 80% of enclosed energy in 1 pixel over ~80% of the field.
- **LR slicer unit** gives 80% of enclosed energy in 1 pixel over ~100% of field
- **Fore-optics** (LR and HR) gives ~100% energy within slice width

The design is quite adequate for the purposes of this study. Improvements are expected in the final design for which an improved figure of merit will be proposed. Recall that the geometrical spot diagrams represent the worst case since they make pessimistic assumptions about the distribution of light in the pupil. Furthermore, the effect of diffraction will dominate over the purely geometrical energy distributions at some wavelengths.

## 8.5 PRODUCTION ISSUES

The best choice of method for manufacturing the optical surfaces is to diamond turn metal or appropriate composite materials. Since this material can be thermally matched to the material of the instrument mounting, it will help to remove thermal expansion differentials. Diamond turning of large aspheric optics is routine for infrared instrumentation. The innovation required here is to apply the same technique to small segmented optics.

The requirement is for a modest number of mirrors each with a large numbers of (mechanically co-aligned) facets. Diamond turning will permit these surfaces to be an arbitrary asphere of revolution (subject to certain dimensional limits). The current design uses mostly spheres and toroids. The use of aspheres will improve the image quality.

The basic principles of manufacture have been tested by a *Proof of Concept* (POC) made by *Precision Optical Engineering Ltd (POE)* for the University of Durham. A more advanced prototype is being manufactured at POE under contract with LAS.

## 8.5.1 Proof of concept results

The POC consists of 20 co-aligned spherical slices with a small angular deviation between them (Figure 19). This is intended to simulate the slicing mirror which we consider the most difficult to make. The slice width is 0.5mm which is somewhat thinner than the width we would actually require for NGST-IFMOS (~0.9mm) and so represents a worst-case problem. The diamond machiner at POE is shown in Figure 20.

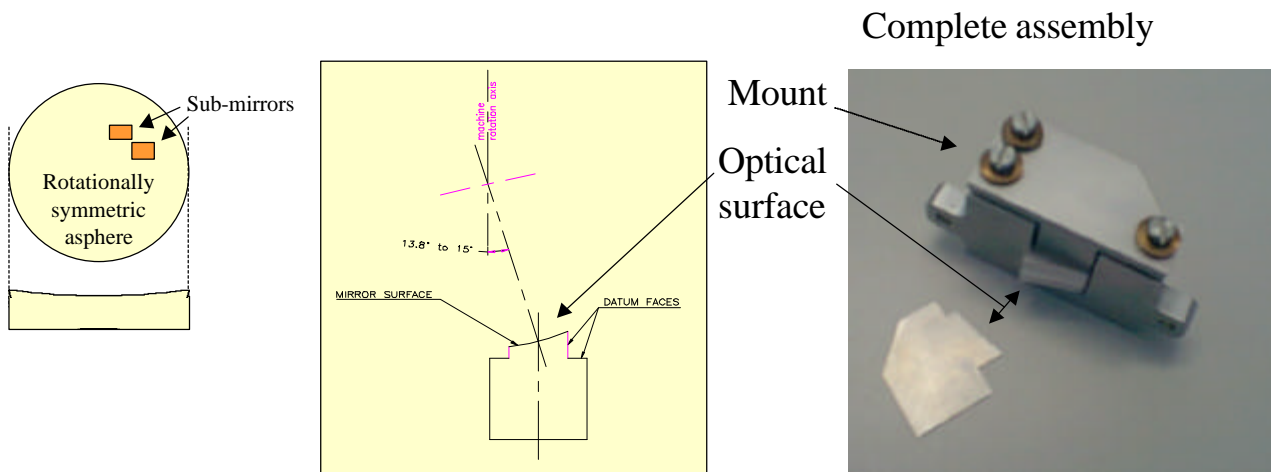


**Figure 19:** Illustration of Proof of Concept. Left: layout on the vacuum chuck which allows arbitrary figures of rotation to be generated. Centre: definition of the centre of curvature of the spherical surface. Right: picture of assembled POC.

Profilometry shows that excellent surface smoothness has been obtained with a RMS roughness of 11nm. This is already good enough for NGST IFMOS since predictions of the *total scattered light intensity* for 6 reflections indicate an *upper limit* to the throughput loss of only a few percent at short wavelengths. This is pessimistic since scattering from surfaces conjugated to the image will not result in the full amount of light loss implied by the scattering estimate.



**Figure 20:** Picture of POC slices on the vacuum chuck at POE. The diamond tool can be seen at the extreme right.

## 8.6 ESTIMATED THROUGHPUT OF INTEGRAL FIELD UNIT

The throughput of the integral field unit (fore-optics plus slicing unit) alone may be estimated as shown in Table 8.

**Table 8 :** integral field unit throughput

l (mm)	<i>Diffraction</i>		<i>Scattering</i>	<i>Total</i>	
	T(HR)	T(LR)	T	T(HR)	T(LR)
1.25	0.97	0.96	0.94	0.82	0.82
1.875	0.95	0.93	0.97	0.83	0.82
2.5	0.93	0.91	0.98	0.82	0.81
3.75	0.90	0.85	0.99	0.80	0.77
5.0	0.89	0.80	1.00	0.80	0.73

This assumes the appropriate beam characteristics for the spectrographs described elsewhere and that each surface has a reflectivity of 98.5%, appropriate for gold coatings. Note that these predictions are pessimistic since the upper limit to the scattering loss (described above) has been assumed.

## 8.7 REFERENCES

- Content, R., 1997. SPIE 2871, 1295.  
 Content, R., 1998. SPIE, 3354, 187.  
 Krabbe, A, Thatte, N., Kroker, M., & Tarconni-Garman, L., 1997. SPIE 2871, 1179.

## 9 SPECTROGRAPH OPTICAL DESIGN

### 9.1 OVERALL PRESENTATION

The design is based on TMA (Three Mirror Anastigmat) systems. The low resolution channel have one collimator with one camera per wavelength octave, one 1.25-2.5 microns blue camera, one 2.5-5 microns red camera. The high resolution channel is based on a double pass spectrograph.

Because of the effect of diffraction on each of the slicer slices, the pupil of the spectrographs are oversized in the dispersion direction in order to minimize light losses. The speed of the camera is limited to F/2.5 in order to avoid manufacturing and integration difficulties.

The designs have been produced assuming 2kx2k detectors, with 18 microns pixels.

### 9.2 LOW RESOLUTION CHANNEL

The low resolution channel is based on one collimator and 2 cameras (one per octave, see Figure 21). Two prisms are used as dispersive elements, this gives high efficiency and avoid order overlap problems. The two channels are split by a dichroic set on the first face of a prism. The focal plane contains one 2k x 2k detector per camera/octave.

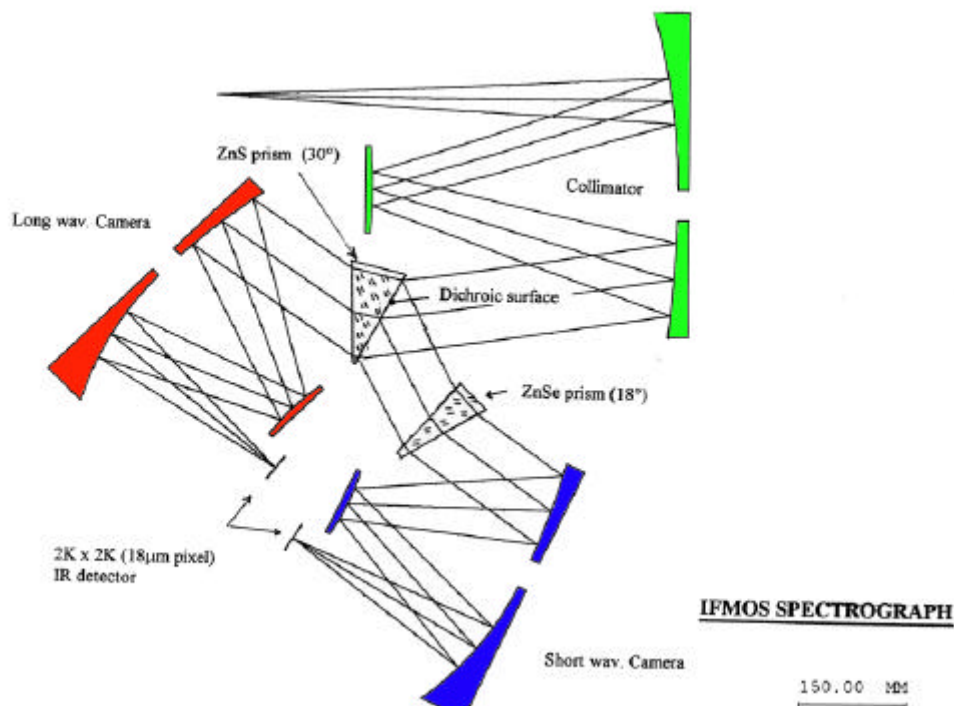
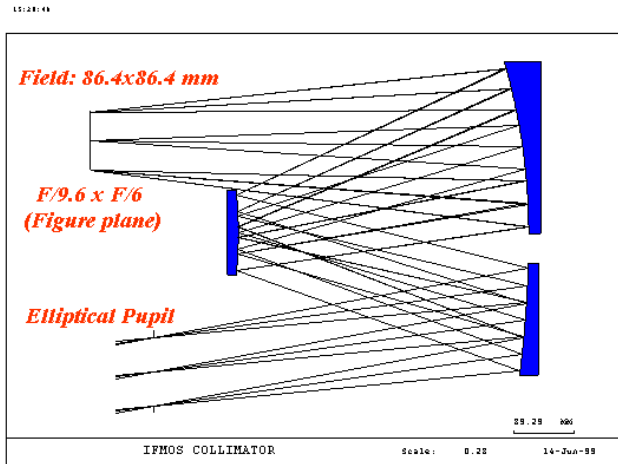


Figure 21: overview of one low resolution spectrograph

LR collimator (Figure 22): The collimator is a F/9.6 x F/6 optics, with a field of view 86.4 x 86.4mm. It is based on a TMA system. The general tolerances are 0.1mm in decenter, and 1 arcmin in tilt. All mirrors are aspherical, but the difference from the best sphere and the slope are not critical for manufacturing.

LR cameras (Figure 23): The blue and red cameras are identical:

- . Entrance pupil: 100 x 160 mm.
- . Camera speed : F/4 x F/2.5.
- . Field of view: 36 x 36 mm (2K x 2k pixels)



**Figure 22:** LR Collimator

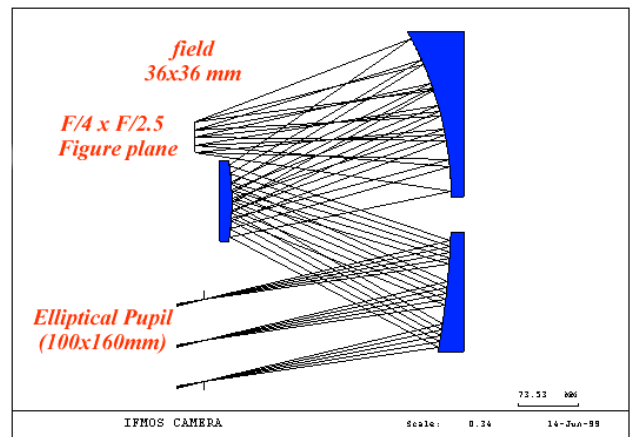


**Figure 23:** LR camera

## 9.2.1 Dispersive elements

The first face of the first prism has a dichroic, splitting the blue and red channels. This allows to optimize the coating of the cameras for each wavelength domain, and use detectors with high wavelength cut-off tailored to the wavelength range of each of the blue and red channels (Table 9).

**Table 9:** Prisms Characteristics

Channel	Wavelength	Prism Angle	Material	Resolution
Blue	1.25 – 2.5 $\mu\text{m}$	18°	ZNSE	77 to 275
Red	2.5 – 5 $\mu\text{m}$	30°	ZNS	125 to 225

## 9.2.2 Optical quality

The overall quality of the spectrograph is excellent, all within 1pixel on the detector, as shown in Figure 24.

## 9.3 HIGH RESOLUTION SPECTROGRAPH

The high resolution spectrograph uses one TMA module in double pass (Figure 25). The collimator provides a small F-ratio adaptation. A folding mirror is included in order to accommodate the entrance slit.

With only one spectrograph, we need 2 gratings on an exchanging device to optimize the throughput vs. wavelength. The spectral resolution obtained is 3000. The pupil size is 166 x 74 mm. A grating with 85 grooves per mm is necessary to achieve the R~3000 in the blue channel.

The focal plane is made of 4 detectors (4kx4k pixels in total).

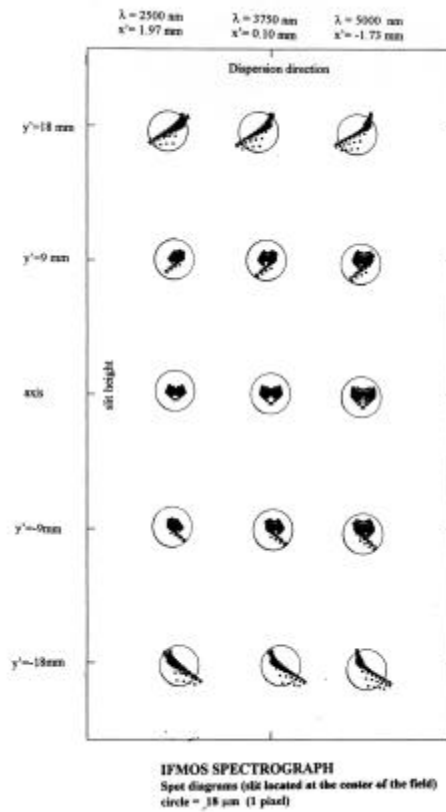


Figure 24: Image quality at the field center (circle=18microns)

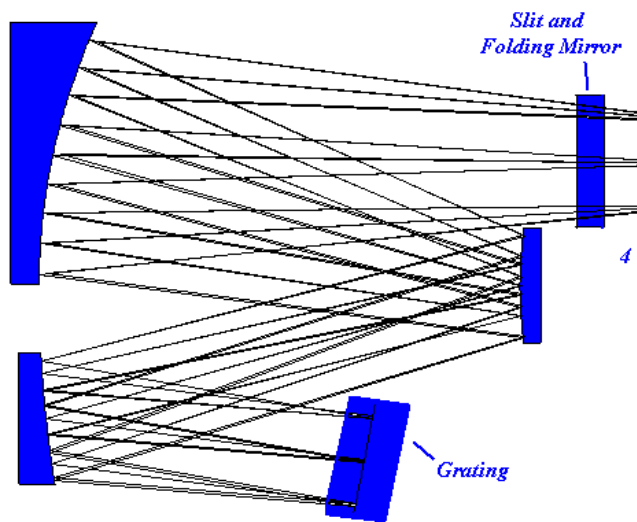


Figure 25: Side view of the HR spectrograph

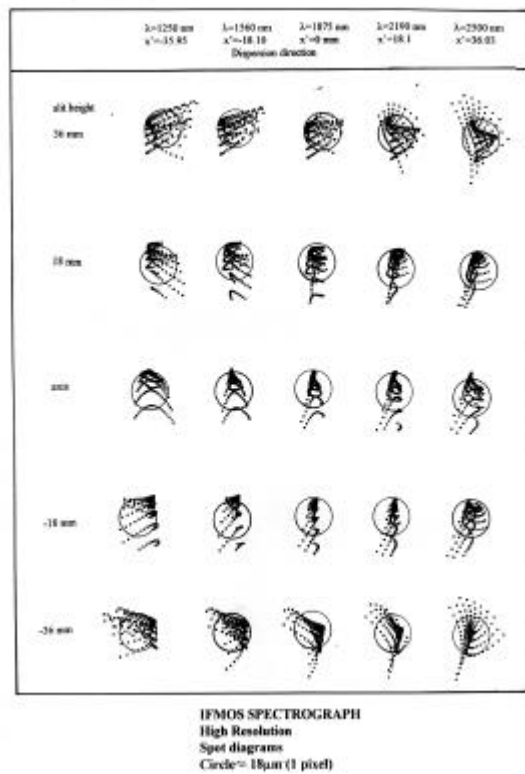


Figure 26 : image quality with the HR spectrograph (circle = 18 microns)

## 10 PERFORMANCE EVALUATION

### 10.1 DESIGN PERFORMANCE

The IFMOS spectrograph performances advantages are listed in Table 10.

**Table 10 : performances advantages**

Wavelength coverage LR mode	1.25-5 microns in one shot
Field LR mode	46x40 arcsec <sup>2</sup>
Spatial sampling LR mode	0.19 arcsec
Wavelength coverage HR mode	1.25-2.5 or 2.5-5 microns
Field HR mode	3.8x2.6 arcsec <sup>2</sup>
Spatial sampling HR mode	0.05 arcsec
Throughput	~60%
Diffraction losses	~5%
Multiplex capability	High: All objects in field of view
Slit losses	None
Geometry constraints: overlap of slits / spectra	None
Background subtraction	Better than 0.1% accuracy, use spectroscopy equivalent to shift-and-add imaging techniques
Imaging requirements	None: not necessary to know properties like magnitude, shape, color, etc. to pre-select
Operations (pointing, offset, etc.)	Easy, 0.1 arcsec accuracy required
Serendipitous discoveries capability	High, no pre-selection of targets

### 10.2 EXPOSURE TIME CALCULATOR, LIMITING MAGNITUDES

An exposure time calculator has been built using the optical design and estimate of throughput. It includes specifically :

- . The number of mirrors of each configuration (LR and HR)
- . The efficiency of prism (LR) and grating (HR)
- . The loss due to diffraction as function of wavelength
- . The detector performances (5 e-/pixel readout noise, 0.02 e-/pixel/sec dark current)
- . The sky background as function of wavelength
- . The IFMOS intrinsic background emission as function of wavelength and temperature

To limit the cosmic rays impacts to less than 2% of the total number of detector pixels, we have assumed a maximum of 1000 sec integration time. Longer exposure time are achieved by co-adding frames and adding variance noises. For point like objects, the number of pixels that are within a 95% encircled energy of the telescope PSF (assumed to be diffraction limited at 1.5 μm)

are computed and co-added. Note that the derived S/N is a lower limit in that case, as it would be possible to perform an optimal summation.

Results are given in Table 11 in terms of limiting magnitude to reach a S/N of 5 per spectral pixel (half the spectral resolution) both for a point source. Two integration times are presented, an elementary exposure of 1000 sec and an equivalent of 10000 sec obtained by coaddition of 10 exposures of 1000 sec. The relative fraction of variance noises are given in each case.

**Table 11 : IFMOS limiting magnitude**

Config	AB mag	Noise Fraction (%)			
		Object	Sky	Dark	Readout
<i>1000 sec integration time, S/N=5 per spectral pixel</i>					
LR	26.9	34	46	9	11
HR	24.2	52	0	21	27
<i>10x1000 sec integration time, S/N=5 per spectral pixel</i>					
LR	28.3	12	61	12	15
HR	25.7	21	1	35	43

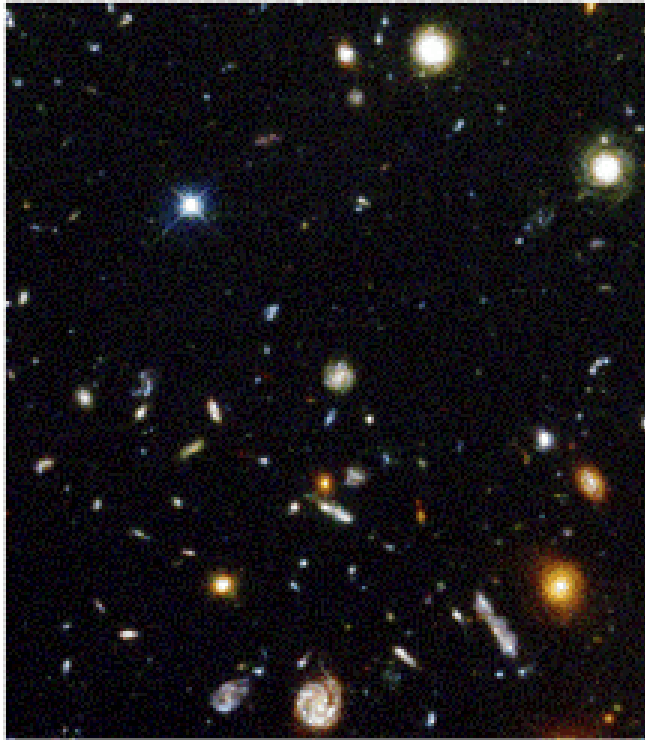
Note that the LR mode is essentially photon noise limited as the detector noise contributes at most to 27% of the total noise in a long exposure (10000 sec). On the contrary, the HR mode is detector noise limited with as much as 78% of noise contribution in a long exposure.

### 10.3 PERFORMANCE SIMULATION: OBSERVING FAINT DISTANT GALAXIES FROM THE HUBBLE DEEP FIELD NORTH WITH NGST-IFMOS LR MODE

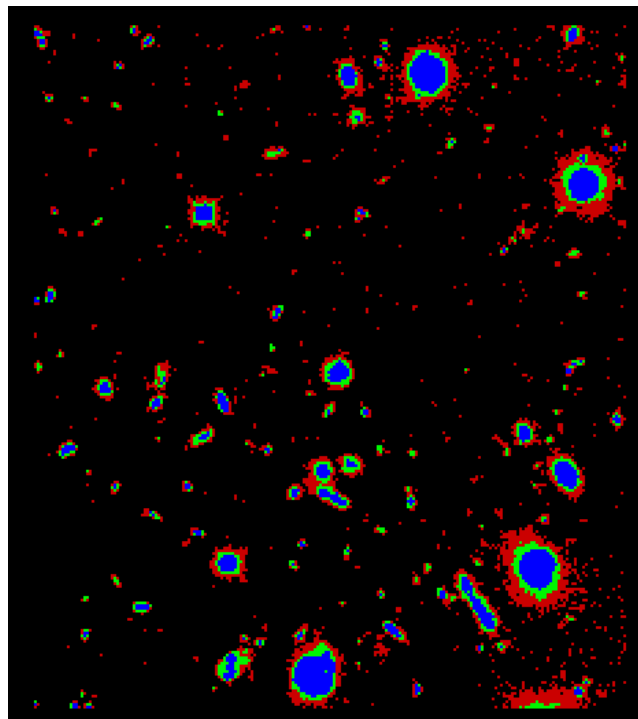
One of the top priorities of the NGST design reference mission is the spectroscopic study of distant galaxies. To highlight the IFMOS capabilities in that field we have simulated how it would perform in the spectroscopic study of the HDF North.

Figure 27 presents one exposure with the LR IFMOS mode. Note that with its field of view of 40x46 arcsec<sup>2</sup>, one IFMOS LR exposure already embraces a large number of objects. As it is now well known a significant part of these galaxies display irregular structure not easily covered with long slit or aperture spectroscopy. With its sensitivity IFMOS would be able to obtain spectroscopic information on ~80 objects in a 10,000s integration time (split in 10 individual exposures of 1000s to avoid cosmic rays contamination). The 1200 spatial pixels for which IFMOS will achieve a S/N larger than 5 *per spectral element* are blue coded in Figure 28. Note that most of the objects will have more than one resolved spatial element. For bright enough objects, spatially resolved spectroscopic studies are then possible. For the faintest ones, a posteriori summation of spatial pixels will allow to maximize the S/N, thus avoiding the classical slit losses of a slit spectrograph.

Another way to improve the detection limit is to sum pixels over the wavelength direction. The limiting magnitude as well as the corresponding number of pixels with S/N larger than 5 per spectral element are given as a function of the resolving power (Figure 29). For example, co-adding all spectral elements, IFMOS reaches a limiting AB magnitude of 31.2 for a point-like source in 10,000s integration time (or 27.6 AB magnitude arcsec<sup>-2</sup> for an extended source). In Figure 28 the pixels with S/N>5 per spectral element are color coded according to the achieved spectral resolution for three typical cases: five colors broad band images (i.e. photometric redshift) in red, a R=30 with 40 spectral elements in green, and the original R=150 spectral resolution in blue. Note that the fraction of pixels with useful spectral information increase rapidly when the resolving power decrease: it ranges from 2% of the total number of spatial pixels at R=150 to 24% for the equivalent broad band image.



**Figure 27** : part of the HDF North with IFMOS sampling (0.19 arcsec) and field of view (40x46 arcsec<sup>2</sup>).



**Figure 28** : A simulated LR long exposure (10x1000 s) of the HDF north. For each pixels shown in that figure the corresponding spectrum has a S/N larger than 5 by spectral elements. Blue pixels : original resolving power (R=150, 200 spectral elements). Green pixels : coaddition of 5 spectral

elements giving a resolving power of 30 and 40 monochromatic images. Red pixels : coaddition of 40 spectral elements giving a resolving power of 4 and 5 monochromatic images.

The property of an IFS to allow *a posteriori* optimal extraction of faint sources using co-addition of pixels in spatial and/or spectral dimension is fundamental to maximize the scientific return of the NGST spectroscopic deep fields. Such a long IFMOS exposure would allow *at the same time* photometric redshifts measurements of very faint sources (30.4 AB magnitude), full R=150 spectral resolution of AB=28.3 sources and spatially resolved spectroscopy of brighter objects. Using multiple dithered exposures and appropriate recombination algorithms it would be possible to achieve very accurate background subtraction and to improve the spatial resolution as it has been done for HST deep images. Contrarily to MOS exposures that need pre-selection of sources according to some a-priori criteria, NGST IFMOS data are fully self consistent and it is likely that the scientific return improves with time as new extraction algorithms are being developed for specific needs.

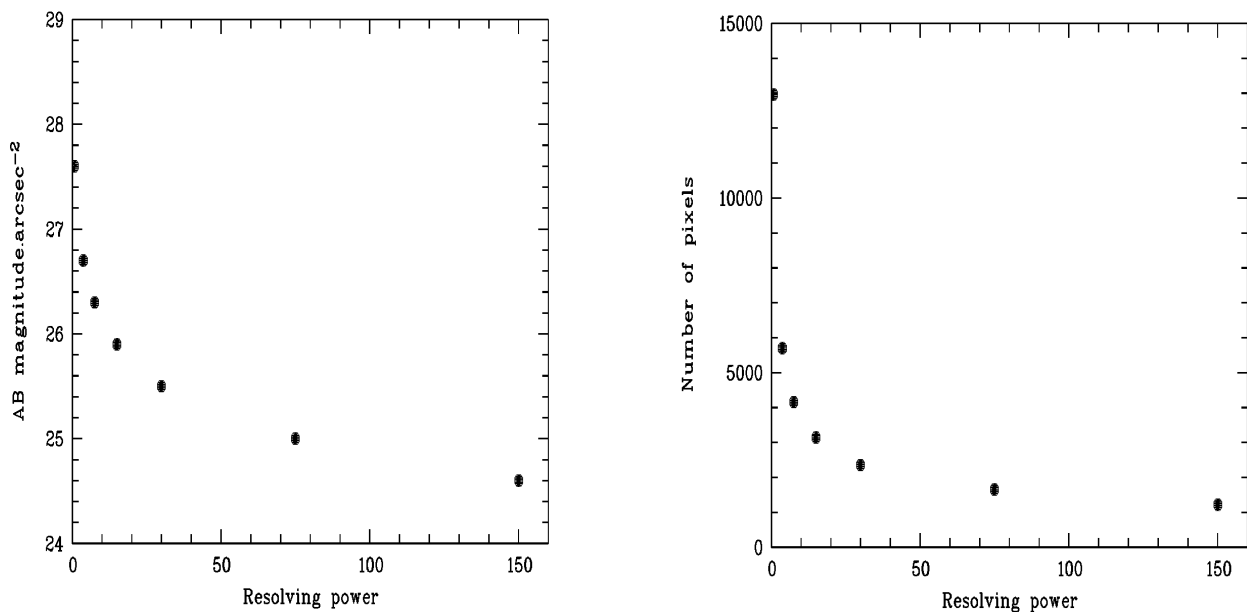


**Figure 29:** Spectral resolution and limiting magnitude. Left panel : limiting surface AB magnitude (S/N=5 in 10 exposure of 1000s) as function of the resolving power. Right panel: Number of active pixels (with a S/N > 5) in the corresponding exposure.

## 10.4 OVERALL EFFICIENCY

Efficiency is a complex number, but ultimately leads to a single factor of merit: time to completion of a given program. We list in

Table 12 the parameters which have to be taken into account when comparing spectrograph concepts, and our assessment vs. 3 existing spectrograph concepts for the NGST. Given the figure of merit above, efficiency gains because of a large field of view can be almost completely offset by e.g. slit losses and geometric limitations on spectra layout.

**Table 12** : parameters entering efficiency comparisons between spectrograph concepts

Property	IFMOS	MOS	FTS
Instrument throughput / diffraction losses	++	+	++
Field of view AND simultaneous wavelength coverage	+	++	-
Slit losses (faint objects)	++	-	++
2D mapping ability	++	-	++
Velocity errors (position of object in slit)	+	-	++
Geometric blending of slits / spectra	++	-	++
Ability for serendipitous discoveries	++	-	++
Background subtraction	++	+	++
Requirements on prior imaging	++	-	++
Operations (setting time, etc.)	++	-	-
Calibrations / stability	++	+	-
Reliability	++	+	+

*Instrument throughput / diffraction losses:* photon losses can occur because of a large number of optical surfaces, coatings, or through diffraction losses. The beam of a spectrograph needs to be enlarged in case of multi-slit spectrographs in order to minimize diffraction losses.

*Field of view AND simultaneous wavelength coverage:* the allocation of a fixed amount of detector pixels is done between spatial and spectral pixels. Larger spectral resolution will decrease the field of view or reduce the simultaneous wavelength coverage. Wavelength

*Slit losses (faint objects):* slit losses will occur for objects with dimensions exceeding the slit width (Figure 31). Adjusting a slit width to an object size is not practical because this leads to degrading the spectral resolution, and spectral resolution varying from object to object. An IFS or FTS spectrograph do not have any slit losses and allow a posteriori optimum extraction.

*2D mapping ability:* the geometry of a slit is not adapted to complex geometry or the presence of small companions close-by the main target. An IFS is designed to obtain spectra of all elements in a 2D area.

*Velocity errors (position of object in slit):* with multi-slits defined by e.g. micro-mirror arrays, the MOS slit setting is done using discrete slit settings spaced e.g. every 0.1 arcsec. Astrometry and setting errors combined with this discrete behavior will introduce positional errors  $\sim 1/2$  of the slit width. This in turn leads to velocity errors which can be as large as a full spectral resolution element.

*Geometric blending of slits / spectra:* a multi-slit layout does not allow to observe all objects in the field in only one setting. Some objects cannot be selected because their spectra would overlap with the spectra of other objects (Figure 30). Depending on the clustering properties and the crowding of the objects, it might be necessary to use 3 to 5 times more settings with a MOS to reach  $\sim 90\%$  completeness. An IFS or an FTS require using only one setting.

*Ability for serendipitous discoveries:* a MOS requires a priori knowledge of the position and properties (e.g. photometric) of objects in the field to be able to position slits on target. Only objects which can be easily seen will then be selected. Objects with e.g. narrow emission lines on a very faint continuum may not be selected: a spectrograph can detect narrow emission lines 5 times fainter than a broad band image would. By observing all objects in the field an integral field spectrograph therefore allows unbiased observations.

*Requirements on prior imaging:* An IFS or and FTS can be set directly into a new field to get spectra, while a MOS requires prior imaging. To avoid biases in target selection, imaging

samples need to be 1 magnitude deeper than the spectroscopy limit, which calls for long integration times.

*Operations (setting time, etc.):* the pointing requirements for an IFS are  $\sim 1$  arcsec for the wide field mode, 0.1 arcsec for the high resolution mode. This will be easily achieved with the NGST. A MOS setting requires a pointing accuracy and stability better than  $1/10^{\text{th}}$  of the slit width or  $\sim 0.01$  arcsec.

*Calibrations / stability:* an IFS with few moving parts is calibrated at regular intervals on order of weeks. A MOS will most probably require calibrations for each mask setting. An FTS requires continuous / parallel calibrations

*Reliability:* while both the MOS and the FTS have few moving parts, they contain either a very complex micro mirror array or a interferometer which are single points of failure. IFMOS has only one moving part and can still operate at  $5/6^{\text{th}}$  of the efficiency if one of the LR channels dies.

The effect of some of these parameters is illustrated in Figure 30 and Figure 31.

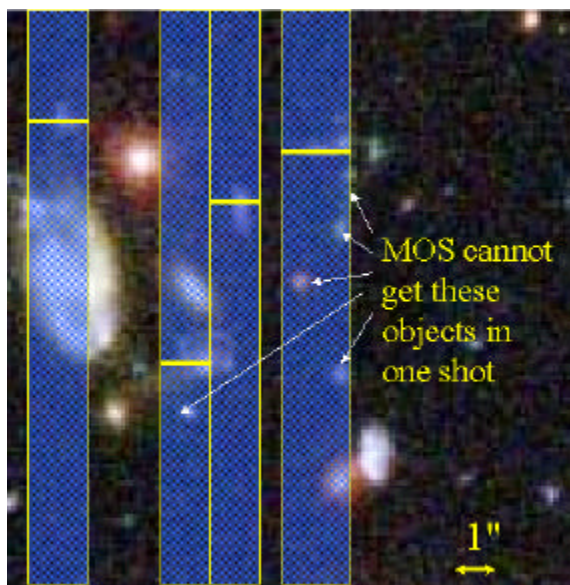


**Figure 30 :** geometric limitation of a multi-slit spectrograph preventing from getting spectra of all objects in a field at once. This limitation forces to multiply the number of slit settings until all objects of interest have been observed, hence with an overall efficiency divided by the number of slit settings

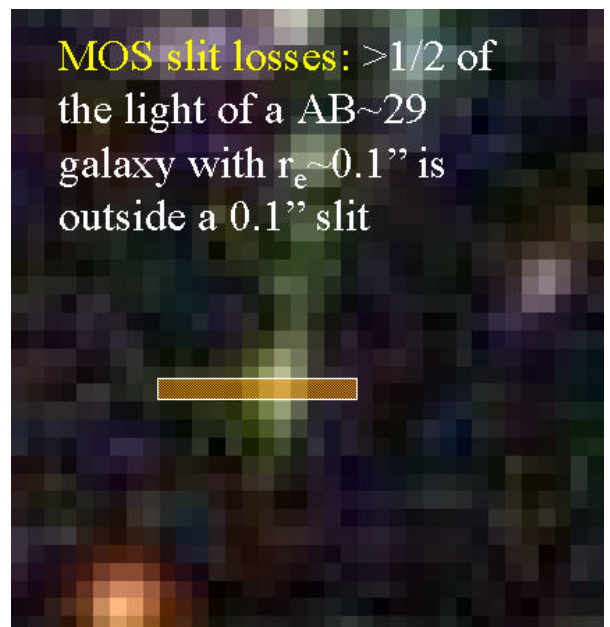


**Figure 31 :** galaxies with AB $\sim$ 28-29 have half light radii on order 0.1 arcsec. A 0.1 arcsec slit introduces light losses of  $\sim 1/2$  the total flux. An integral field spectrograph does not lose any light and allows to use optimal extraction techniques to maximize the S/N. Longer exposure times are thus required for a MOS to reach the same S/N as an IFS. A MOS could have slits with 0.2 arcsec width, but this will compromise the spectral resolution, or the field of view.

## 11 MECHANICAL, THERMAL AND ELECTRICAL DESIGN AND ANALYSIS

### 11.1 INTRODUCTION

DSS has performed the mechanical, thermal and electrical design implementation of the image slicer spectrograph, on the basis of the optical instrument design. The principle instrument design presented in this document evolved after various iteration steps in the course of this study. The main arguments leading to the presented solution are provided.

#### **DSS Study Team:**

The work described in this document has been performed by

- |                                   |                                      |
|-----------------------------------|--------------------------------------|
| . Winfried Posselt                | study management, system engineering |
| . Dietmar Scheulen/Rudolf Sippel  | mechanical engineering               |
| . Herbert Huether                 | mechanical design                    |
| . Armin Hauser                    | thermal engineering                  |
| . Werner Hupfer                   | electrical engineering               |
| . Dr. Robert Buschner-Ueberreiter | detectors                            |

More details on mechanical, thermal and electrical design, detectors and signal processing can be found in the document NGST-DSS-WHRP-001, "General Design Considerations" , written by Dornier ("Woodshole" report).

### 11.2 MECHANICAL DESIGN AND ANALYSIS

#### 11.2.1 General Design Requirements

The following mechanical design requirements evolved in the course of this study:

- . the instrument should combine one High Resolution (HR) and three Low Resolution (LR) spectrographs
- . the overall instrument mass should not exceed 150 kg
- . the first eigenfrequency should be higher than 60 Hz

The dimensions of the four spectrographs are determined by their optical designs, which are based on reflective optics in order to avoid the ageing criticality of certain refractive materials. Task of the mechanical structure is to support the optical components of the spectrographs in the required positions, compatible with the launch and operating conditions.

#### 11.2.2 Design and Material Considerations

##### 11.2.2.1 General Design Considerations

The mechanical design philosophy was to minimize the instrument mass. Moreover, the overall instrument design aims for low criticality during all MAIT steps and respecting the mechanical requirements.

These requirements have been achieved with the following:

- the different spectrographs were arranged in a proper way aiming at maximum compactness of the total configuration: all three LR spectrographs are arranged in three "layers" with no baseplates in between
- the amount of secondary structure was minimized: most of the optical components were mounted directly to the primary structure
- the panels, mirrors and support structures are made of C/SiC and light-weighted; a high specific bending stiffness was achieved by triangular cavities rimmed by edge flanges

## 11.2.2.2 Material Selection

The decisive argument for the material choice is the requirement to provide a CTE as low as possible for the mirrors and the connecting structure in view of the large temperature change during cool down from RT to 30 K. It is rather difficult to predict the thermally induced deformations of the different mirror shells if they are made of a material with large CTE like Al or Be. In addition, Al mirrors need a special coating and will have a relatively high CTE even at 30 K, and corresponding high sensitivity to thermal gradients. The CTE of Be is lower, but when selected as material for the structure it should consequently be selected also for all other components (mirrors, brackets, fittings, etc.) with disadvantages on other fields like toxicity, availability, cost, etc.

Therefore, C/SiC is the selected baseline material for the instrument structure and the mirrors.

## 11.2.3 Baseline design Description

### 11.2.3.1 Instrument design

The baseline overall design is shown in Figure 32 to Figure 34. The mechanical design implementation of the optical configuration can be seen in Figure 32. The primary structure consists of a top and a bottom plate, which are connected by several vertical plates. At different locations the structure is stiffened by struts and smaller connection plates. The complete primary structure is made of C/SiC material. All panels are extensively (~ 90%) light-weighted by triangular cavities. The back edges of the remaining ribs are reinforced by flanges, which provide the high plate bending stiffness.

The three LR instruments are arranged in a stack on top of each other between the top and bottom plates, as can be seen in Figure 33. The optical components of the LR spectrographs are mounted to the vertical plates, only few secondary mounting structures are needed in this configuration.

The components of the HR instrument are mounted to the backside of one vertical plate (Figure 33). For this instrument the components are directed normal to the mounting plate and hence the secondary mounting structures for this spectrograph are larger and heavier.

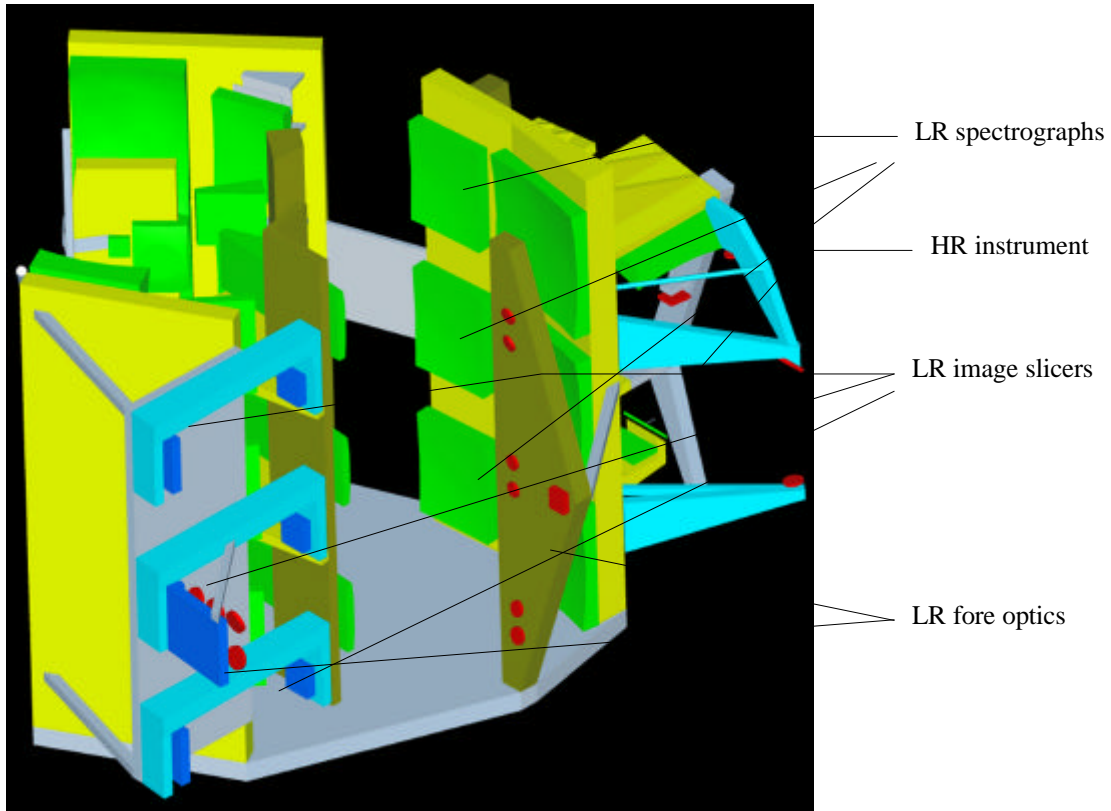


Figure 32 : opto-mechanical implementation of the optical design (top plate taken off)

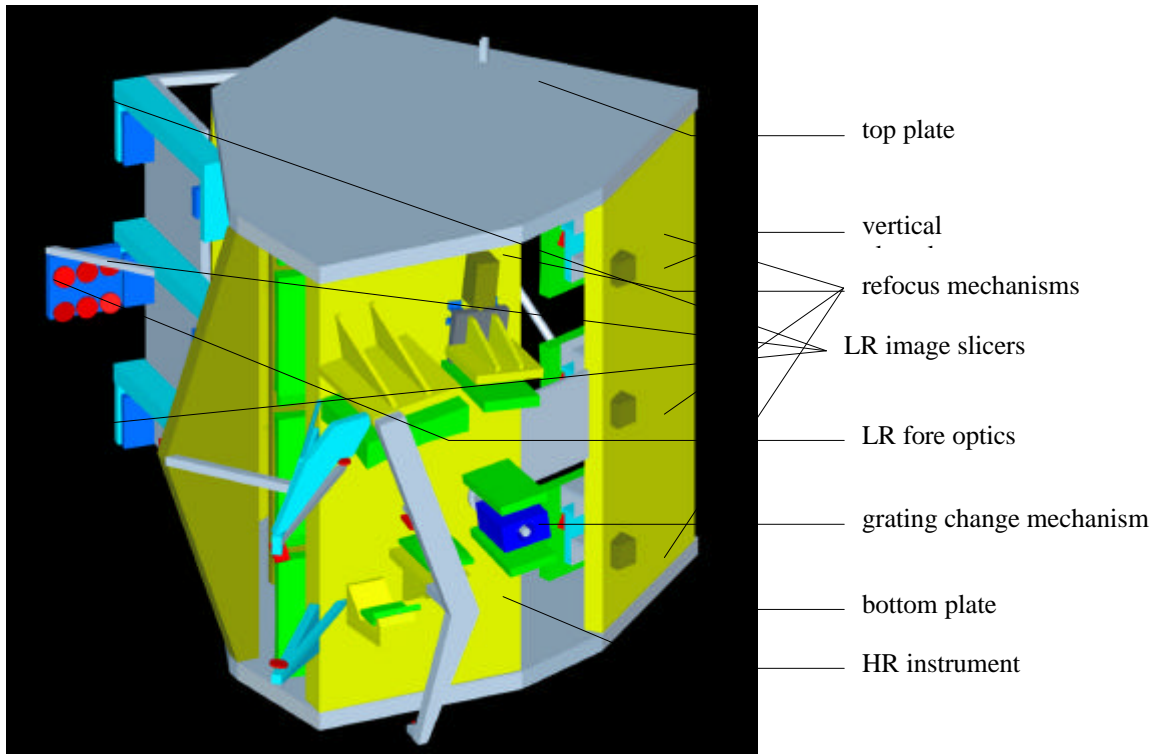
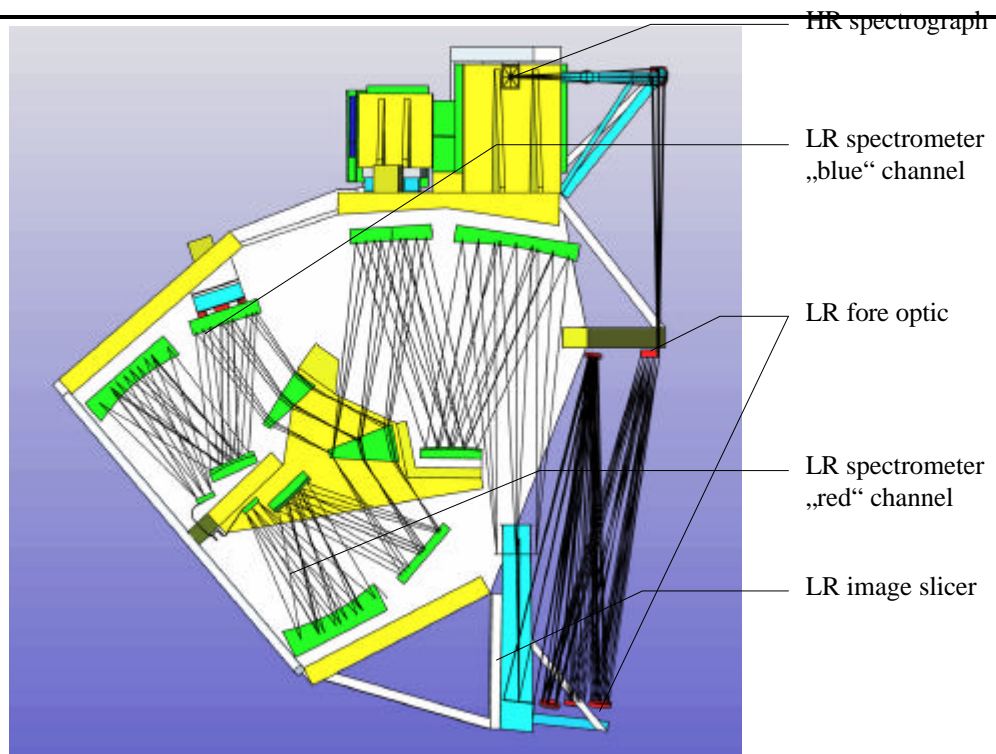


Figure 33 : complete instrument with view on HR spectrograph



**Figure 34** : top view of LR spectrograph showing the vertical panels

### 11.2.3.2 Mounting Techniques

The instrument fore-optics and spectrometer units consist mainly of mirrors. The principle mounting and light-weighting techniques of these elements are shown in Figure 35. Large mirrors are fixed by isostatic 3-point-mounting with flexible INVAR mounts. Smaller mirrors are fixed by a slotted central INVAR tube.

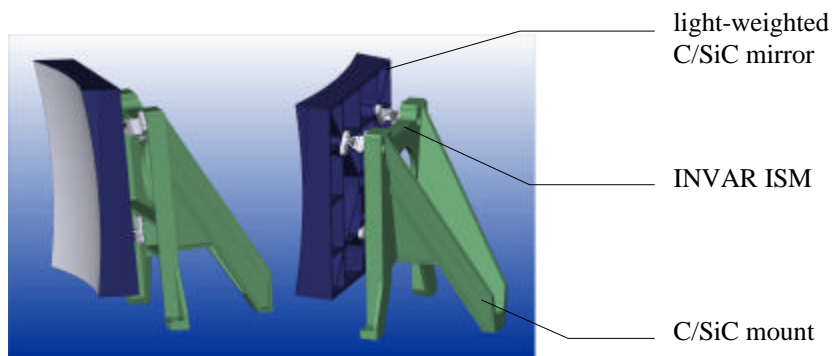


**Figure 35** : principle of mirror light-weighting and mirror mounting

The instrument interface to the ISIM will also be realized by isostatic mounting to decouple from the thermal deformations between the connected structures. As connection elements flexible mounts are foreseen. Favorite materials for the flexible mounts are INVAR, titanium or CFRP, depending on the magnitude of the imprinted loads and deformations.

### 11.2.3.3 Mechanisms

The correct focussing of each spectrograph can be adjusted by means of a refocus mechanism, actuating on the position of one spectrograph mirror. This refocussing actuator can be a sequential working linear inchworm type, which is currently under development at Burleigh Instruments for NGST and is already working as prototype. The essential actuator data are

- . resolution better than 20 nm
- . stroke larger than 6 mm
- . holding force: about 4.5 N
- . heat dissipation: 5 mW during calibration and 0.05 mW during operation
- . size of the prototype: about 50 x 50 x 100 mm

Due to the limited holding force of this actuator type hold down and release mechanisms have to be foreseen, to clamp the refocussing mirrors during launch.

The principle design for the grating change mechanism of the HR instrument is derived from the successfully flown ESA-ISO ISOPHOT filter wheels.

#### 11.2.4 Structural Analysis

As basis for the structural analysis a rough finite element model has been established. The primary structure was idealised by plate and beam elements. The stiffness of the light-weighted plates was simulated by suitably selected homogeneous plate properties. The secondary structure and the optical components were idealised by rigid solid elements. The mass distribution was simulated by adapted material densities. The total mass considered in the model was 127.9 kg. The model was supported by isostatic mounting at 3 points. The shape of the calculated lowest eigenmode is shown in Figure 36. The lowest eigenfrequency of 69.7 Hz exceeds the minimum required eigenfrequency of 60 Hz.

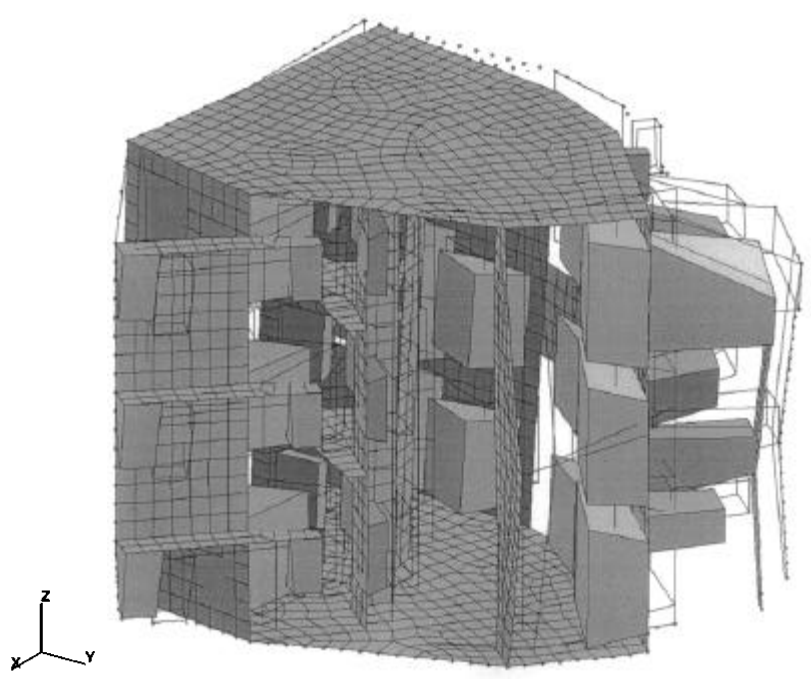


**Figure 36 :** normal mode 1 (69.7 Hz)

Accelerations of 30g in x-, y- and z-direction were analyzed as static load cases. The calculated VON MISES stress values (Table 13) show that the allowable stresses are exceeded in the small areas close to the load introduction points of the instrument structure (interface to ISIM). At these locations the panels have to be suitably reinforced. In the remaining structure the stress levels are uncritical.

**Table 13:** maximum VON MISES stresses in the primary structure due to static acceleration loads

structure area	load case		
	30g in x-direction	30g in y-direction	30g in z-direction
close to load introduction points	260 MPa	120 MPa	158 MPa
in remaining structure	64 MPa	17 MPa	46 MPa

## 11.2.5 Budgets

The overall dimensions of the optical module are 1360 x 1300 x 1050 mm<sup>3</sup>. The mass of the conceptual instrument design is summarized in Table 14.

**Table 14 : mass budget**

primary structure	73.9 kg
LR prisms with support structure	20.7 kg
other LR optical components with ISMs and support structures	26.7 kg
HR optical components with ISMs and support structures	7.0 kg
total structure mass of optics module (no margins)	128.3 kg

Additional components like interface and connector brackets, baffles, launch lock and release mechanisms, thermal insulation, focal plane units and harness amount to approximately 15 kg. The estimated overall mass of the instrument within the ISIM is ~ 145 kg. This mass does not include the ISIM external instrument electronics.

## 11.3 THERMAL DESIGN AND ANALYSIS

### 11.3.1 Thermal Requirements and Assumptions

The IFMOS instrument contains 10 large detector arrays with an average dissipation of 14 mW. The dissipation of the grating change mechanism, which is operated infrequently, is assumed to be about 0.5 mW. The detectors require an operating temperature of . 30 K and shall be passively cooled by the ISIM radiator system. The total IFMOS heat load budget shall not exceed 50 mW. The IFMOS instrument baseplate temperature is assumed to 35 K.

The following assumptions are taken to calculate the parasitic heat load across the different harness paths (see also §6):

- . Harness to FPU (30 K): 480 stainless steel wires with 0.1 mm diameter, 2 m length and thermalized at 100 K
- . Harness to mechanisms (35 K): 46 stainless steel wires with 0.5 mm diameter, 2 m length and thermalized at 100 K
- . Harness to sensors (35 K): 60 stainless steel wires with 0.1 mm diameter, 2 m length and thermalized at 100 K

## 11.3.2 Passive Cooling Concept and Performance

Assuming a radiator area of 8.25 m<sup>2</sup> (2.5m x 3.3m, tbc), the total radiator heat rejection capability at 30 K is about 320 mW and the parasitic heat load share into the ISIM is nearly 100 mW. Thus, about 220 mW remains for the instruments power dissipation at a radiator temperature of 30 K.

A more detailed description is given in the document "NGST-ESA payload study – General design considerations" NGST-DSS-WHRP-001.

## 11.3.3 IFMOS Thermal Design Principle

The principle design of the IFMOS thermal concept is shown in Figure 37. Each detector array is mounted separately onto the warmer instrument structure by means of a thermal decoupling device and thermally connected to a thermal bus bar using a high purity Aluminum or copper cooling strap. The bus bar is then attached to the ISIM radiator by another flexible cooling strap (not shown). To minimize parasitic irradiation from the warmer environment the cooling straps and the bus bar should have an emissivity of < 0.05, e.g. goldized surfaces.

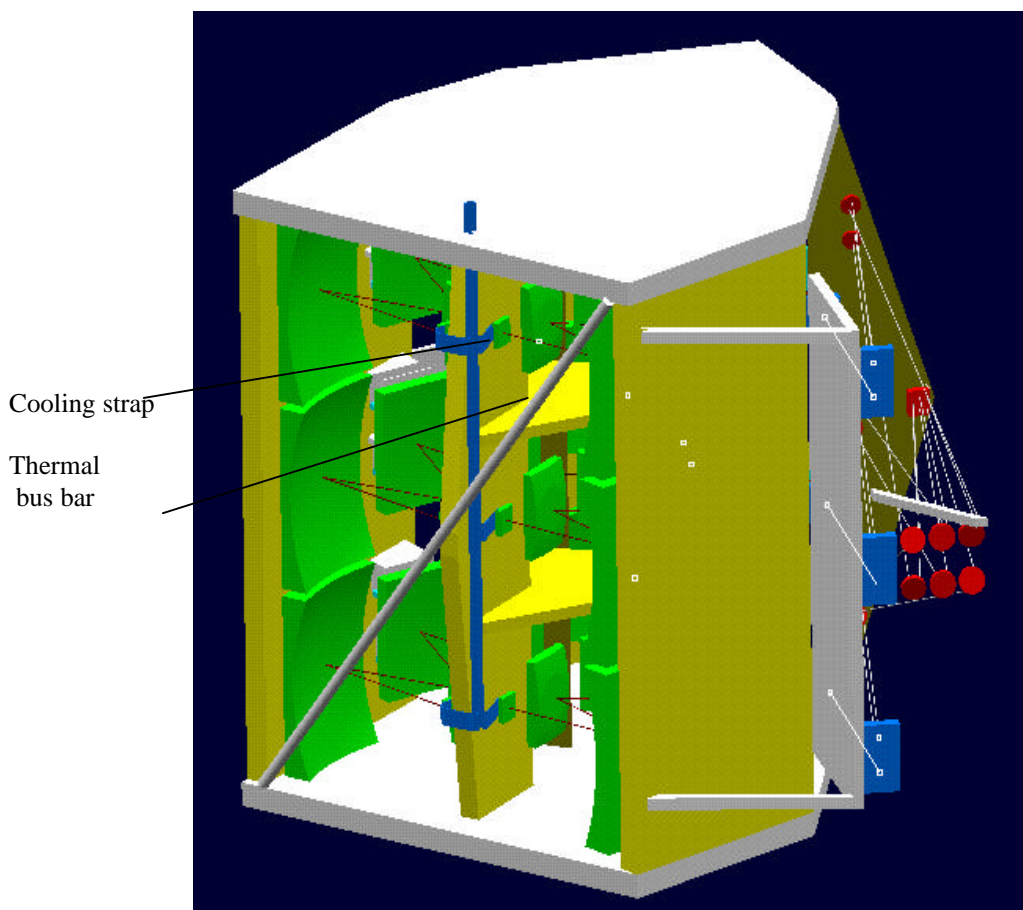


**Figure 37 : Thermal Design Concept for IFMOS Detector Cooling**

The size of each detector array is assumed as 35 mm x 35 mm with a mass of about 40 g. The parasitic heat from the instrument baseplate to each detector array has been calculated assuming a thermal decoupling device with a thermal conductance of 0.32 mW/K. For a decoupling device made out of GFRP (Glass Fiber Reinforced Plastic) or Vespel a cross section to length ratio of about 1.8 can be derived.

In total 48 stainless steel wires with 0.1 mm diameter and 2 m length connected to a 100 K thermalization interface are assumed in order to calculate the heat flow across the harness.

For the above mentioned thermal design the following heat loads per detector have been calculated (assumptions: detector operating temperature = 30 K, instrument baseplate temperature = 35 K):

- . average detector dissipation: 1.4 mW
- . parasitic heat across support structure: 1.6 mW
- . parasitic heat across harness (48 wires): 0.1 mW

The detector cooling strap is made out of high purity aluminum or copper band with 1 mm x 30 mm cross section and a low emissivity surface (< 0.05). The length is assumed as 500 mm. The electrical insulation between the cooling strap and the detector can be provided with STYCAST adhesive, Diamond or Sapphire elements. Thus, in total a temperature gradient between detector and the thermal bus bar in the order of 0.1 K can be expected.

### 11.3.4 Heat Load Budget

The overall heat load from the IFMOS to the ISIM main radiator at . 30 K is calculated as following:

Average dissipation of the 10 detectors:	14 mW
Parasitic heat across the detector mounting structures:	16 mW
Parasitic heat across FPU harness:	1 mW
<u>Parasitic heat onto cooling straps and bus bar:</u>	<u>4 mW</u>
Total heat load	35 mW

The dissipation on the IFMOS instrument structure is mainly parasitic heat across the harness which is estimated to 3.0 mW. Another 0.5 mW may be added as average load from the grating mechanism, yielding a total of 3.5 mW.

## 11.4 ELECTRICAL DESIGN AND ANALYSES

### 11.4.1 Detectors

The IFMOS instrument requires detectors which shall cover the NIR range from 1 to 5µm. The corresponding detector requirements are listed In Table 15.

**Table 15: IFMOS Detector Requirements**

Instrument	Range	Detector Size	Pixel Size	Dark Current	Read Noise	Top
	µm		µm	e-/sec	e- rms	K
IFMOS, LR	1 – 5	6 x 2K x 2K	18	< 0.1	< 5	~ 30
IFMOS, HR	1 - 5	4K x 4K	18	< 0.02	< 5	~ 30

For NGST applications these detectors have to fulfil very demanding requirements:

- . very low dark noise
- . very low read noise
- . very low power dissipation
- . very large size of detector array

The most promising detector materials for the NIR spectral range are InSb and HgCdTe.

## 11.4.2 Signal Processing

### 11.4.2.1 Signal Processing Task Overview

The tasks of the instrument electrical system include the acquisition of images with a detector, conversion into analog and digital representation by a signal processing chain, on-board image processing and storage for transmission by the space craft to ground.

A major constraint is the minimization of heat dissipation inside the ISIM. Only essential electrical components are located there. Signal processing electronics is located outside of ISIM on the connecting truss. The IFMOS Scientific Instrument Control (SIC) is located in the Satellite Support Module (SSM).

Figure 38 shows a functional block diagram of the IFMOS instrument within the space craft context and shows important thermal and physical constraints.

IFMOS components located within the ISIM are:

- Focal Plane Unit (FPU) at 30K, consisting of the SCA (Sensor-Chip-Assembly = detector + multiplexer)
- Stepper motor for grating change mechanism with no dissipation in power-off condition
- Inchworm for refocus adjustment with no dissipation in power-off condition
- Hold-down and release mechanism for refocus mirror with no dissipation in power-off condition
- Sensors for temperature, voltage/current, etc.

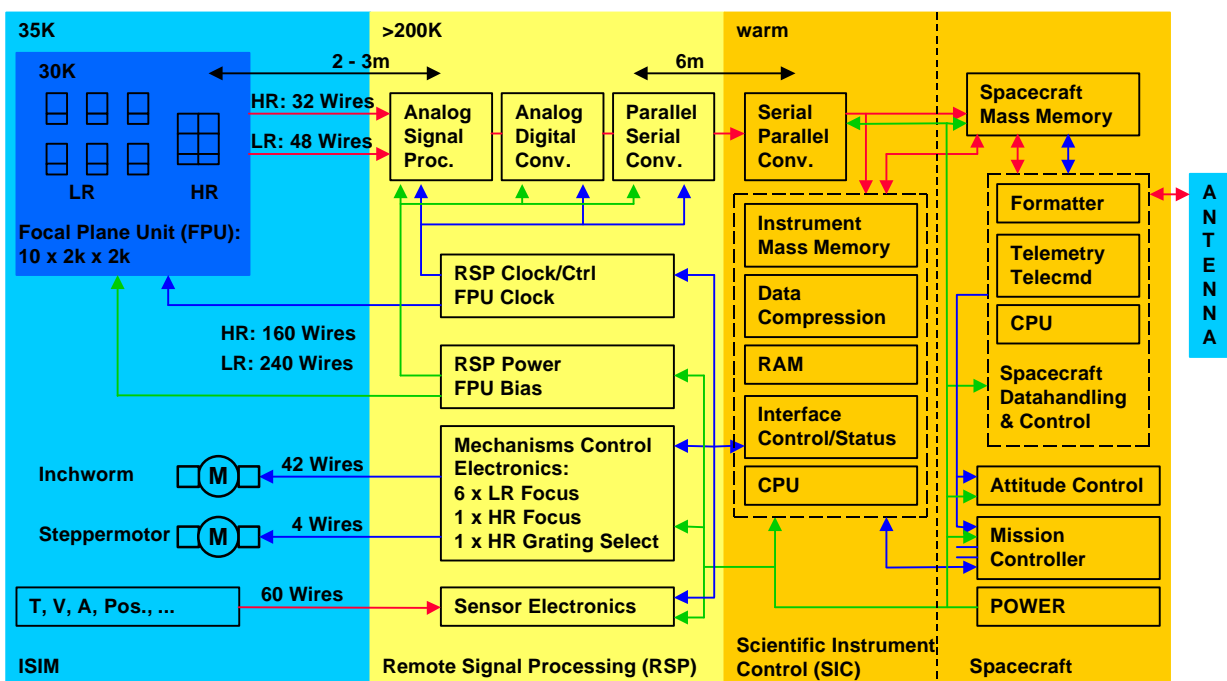


**Figure 38:** Functional Block Diagram

Located on the connecting truss is the Remote Signal Processing (RSP) electronics, which includes the following components:

- Interface to IFMOS SIC: FPU parameters and control, sensor data, main power, mechanism control

- . Internal RSP clock, control and power generation
- . FPU bias and clock generation
- . Analog signal processing of FPU data: preamplifier, filters, impedance matching
- . Analog Digital Converter
- . Parallel/Serial Conversion with high data rate link
- . Mechanism control, may include sensors for position indication
- . Sensor electronics (ADC and serial data link)

FPU/RSP are controlled by the Scientific Instrument Controller (SIC), which performs the following tasks:

- . Space craft interface for reception and processing of Mission Controller (MC) commands and parameters.
- . RSP control (parameters for image acquisition)
- . Mechanism control
- . Reception of digital science data
- . Science data processing and data compression
- . Science data storage

### 11.4.2.2 Analog Signal Processing Design Trades

Please, see the document “NGST-ESA payload study – General design considerations” NGST-DSS-WHRP-001

### 11.4.2.3 FPU Readout Scheme

Please, see the document “NGST-ESA payload study – General design considerations” NGST-DSS-WHRP-00. Figure 39 shows the power and wire estimates for the FPU, mechanics, sensors in ISIM and in RSP.

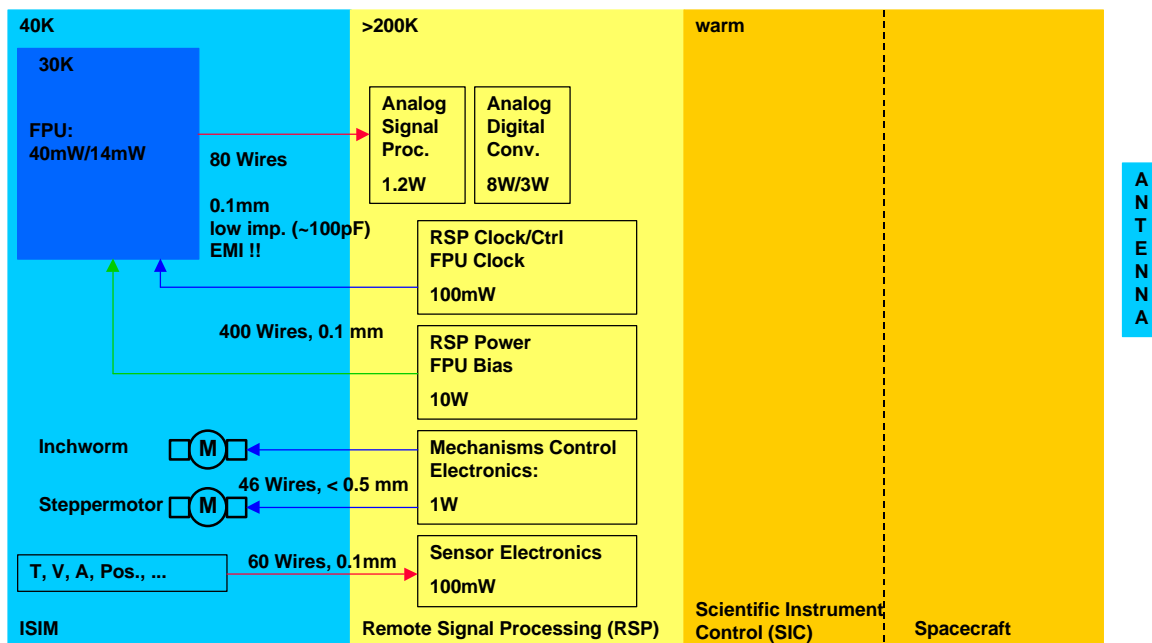


Figure 39: Power Budget and Harness Size

## 11.5 TECHNICAL BUDGETS SUMMARY

The instrument budgets which have been detailed in the previous sections are summarized in Table 16 below.

**Table 16:** Instrument budget summary

Parameter		Estimated budget figure	Requirement
<b>Dimensions</b>	Length (envelope)	1360 mm	
	Width (envelope)	1300 mm	
	Height (envelope)	1050 mm	
<b>Mass</b>	Mass of conceptual design	128.3 kg	
	Mass incl. baffles, brackets, harness, etc.	~ 145 kg	< 150 kg
<b>Eigenfrequency</b>	First eigenfrequency	70 Hz	> 60 Hz
	Second eigenfrequency	121 Hz	
<b>Heat Load</b>	Load on cold radiator	35 mW	< 50 mW
	Load on ISIM structure	3.5 mW	
	Load on truss structure by RSP	14.3 W	
	Load on truss structure by instr. control	1.1 W	
<b>Processing</b>	Processing power	84 Mips	
	CPU clock	100 MHz	
<b>Data Rate</b>	Science data rate	1 Mbps	
<b>Memory</b>	Instrument mass memory	87 Gbit	
	Satellite mass memory (compression ~ 2)	40 Gbit	

## 12 CRITICAL AREAS, DEVELOPMENT NEEDS AND FOLLOW-ON ACTIVITIES

We provide below a summary of potential critical technologies of this instrument concept. It is the goal of this document to identify these technologies in an early stage of the project to allow definition of a dedicated technology development program in order to reduce the development risks of the project.

### 12.1 CRITICAL AREAS AND TECHNOLOGY REQUIREMENTS

The image slicer spectrograph is an instrument concept which will be flown for the first time. Although its principle of operation is already demonstrated in on-ground astronomical instruments, the IFMOS concept contains certain hardware units which have not yet been built to the required dimensions and which have not yet been operated at the foreseen NGST environmental conditions.

Figure 40 shows the HW matrix of the IFMOS spectrograph. Shaded boxes provide an overview of the critical subsystems or of the subsystems containing critical elements, as listed in §12.1.1.

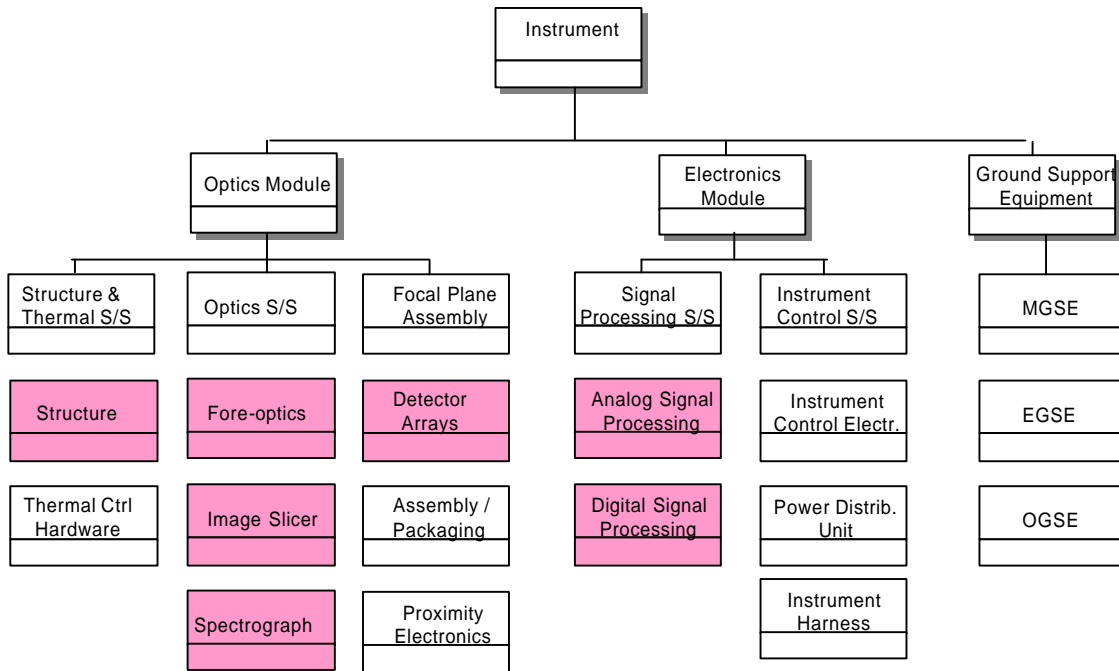


**Figure 40** : Instrument Hardware Breakdown, indicating critical subsystems

## 12.1.1 Critical Areas and Risks

Table 17 lists the potential critical areas identified for the IFMOS spectrograph.

**Table 17** : Potential critical areas of the IFMOS spectrograph

Subsystem	Critical area	Comment
Fore-optics	Alignment and stability of toroidal mirrors under environmental tests	Preliminary analyses show low criticality
	Testing of toroidal mirror surface figure quality	Requires sophisticated test equipment
Spectrograph	Alignment of TMAs	Preliminary analyses show low criticality
	Suspension of prisms	Early verification recommended
	Mechanisms at 30K for refocusing and grating change	Early verification recommended
Image Slicer	Production processes (manufacturing, alignment, handling, testing, etc) for large amount of small optical components (484 pieces, 196 designs)	Early verification recommended
	Suppression of straylight and optical cross-talk	Early verification recommended
Structure	Large dimensions: mass and stiffness critical, sensitive to thermal gradients	C/SiC has high Young's modulus, low CTE and low specific mass, but new technology ⇒ <i>early verification recommended</i> ⇒ <i>define backup solution</i>
	Actual design without sub-structure on functional unit level => critical AIT	Additional sub-structures recommended => increase of instrument mass
Detector Arrays	Low dark current required, especially for HR instrument	Critical for the noise advantage of this instrument concept; but recent tests on InSb detectors promising
	Long distance data transmission w/o preamp: EMI may introduce noise	Eventually preamps for HR channel close to detectors, but increase of thermal load
Signal processing	Up-the-ramp sampling and image processing requires large mass storage	Eventually reduce amount of sub-samples per 1000 sec
	Image processing algorithms (CR removal, etc) depend on in-orbit array characteristics, which are difficult to simulate and may change with time	Requires flexible image processing concept with SW upgrading capability

Potential critical elements to be considered during the development of the instrument are

- . items whose failing may affect the satellite performance or survival probability
- . single point failures and non-redundant major elements
- . items whose failing/degradation may affect the instrument performance
- . items not previously space qualified
- . items with exceptional process sensitivity and long lead items

The critical areas of the IFMOS spectrograph are mainly concerned with the last two items, i.e. structure materials and subsystems which contain new technologies or technologies of expected long development duration.

The listed areas are of different criticality grade. The majority of the listed items can be treated within the standard engineering tasks and may not require dedicated technology developments. However, these items require careful task planning and additional design and/or analysis effort in order not to endanger the overall development schedule.

Some other areas are considered of high criticality, which require an early demonstration of feasibility. Any failure of the proof of concept of these items will require a revision of the conceptual design or even the change towards a completely new design concept.

The two most critical areas identified in this context are:

- . C/SiC Material

This promising material has been developed in the early 1990s and has been used in the OERSTED project. For SEVIRI a 60 cm mirror and a 2 m structure for ground calibration purposes have been developed, built and successfully tested. Further use of this material in space projects is currently under discussion.

The criticality of this material is related to the unknown material parameters at the foreseen low temperature operating conditions and to the lack of experience with corresponding low temperature interface connections. Other materials may be useable in case the behavior of C/SiC is not proven to be adequate

- . Image Slicer Unit

The principle of operation for ground operation has successfully been demonstrated by the MPE, Garching, and there are currently more advanced image slicer spectrographs for ground use under development by University of Durham and Astronomy Technology Center, Edinburgh.

The criticality of the IFMOS design lies within the required size of the slicer units, i.e. the amount of small optical parts to be assembled and to be kept stable during cool-down to operational temperatures. Another point of criticality may arise from the fact that due to diffraction at the edges of the slicer mirrors the beam diameter at 5  $\mu\text{m}$  is somewhat larger than the pupil mirrors, leading to optical cross-talk.

## 12.1.2 Technology Development Roadmap

The IFMOS technology development roadmap for the major critical technologies is depicted in Figure 41. It shows the two main critical hardware elements, the C/SiC material and the image slicer unit, to be developed in an early stage of the project.

It is assumed that the detectors and actuators (for optics refocusing) for NGST will be developed on system level, since these technologies are not instrument specific and will be required for other NGST space hardware units as well.

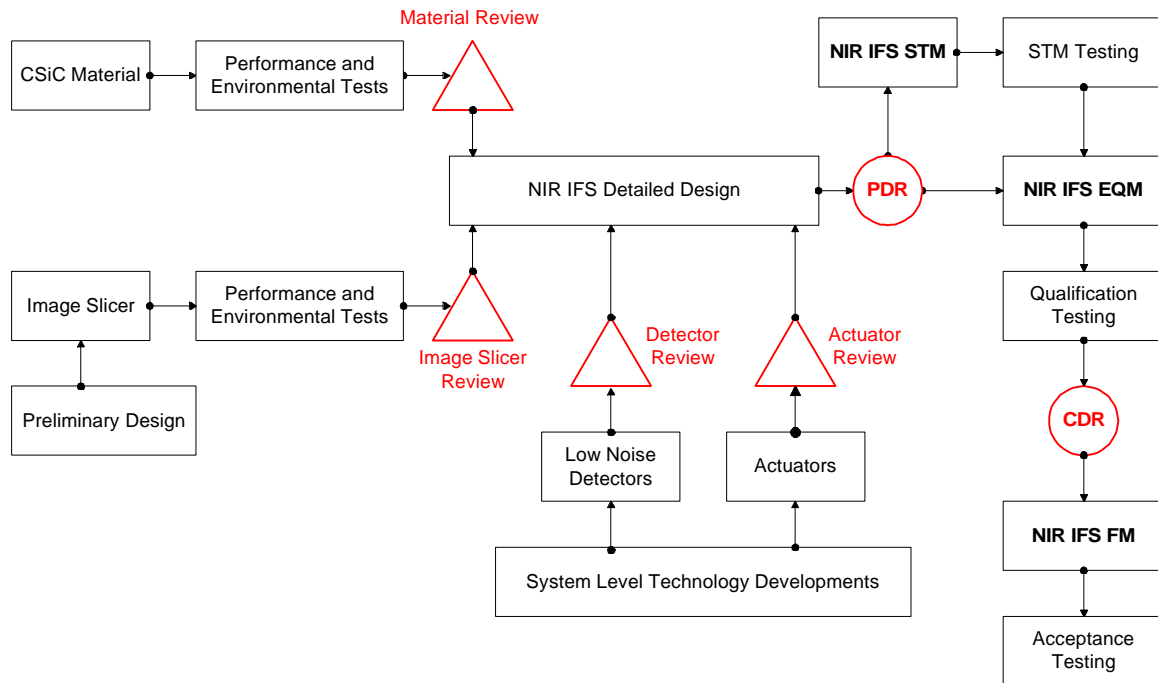


Figure 41 : IFMOS Technology Development Roadmap

## 12.2 RECOMMENDED FOLLOW-ON ACTIVITIES

In order to minimize the development risk certain technology development activities are recommended. Some of these activities are essential for the *proof of concept* and the results should be available prior to further instrument design detailing (ideally prior to Phase A). In the development schedule (ref. §13) these activities are referred to as **Technology Pre-Developments**.

Further development activities are aiming for gain of experience with the new technologies. These activities should be started during Phase A and the results should ideally be available at begin of the detailed design phase (Phase B). In the schedule (ref. §13) these activities are referred to as **Technology Developments**.

### 12.2.1 Verification of C/SiC material for structural and optical components

C/SiC has been identified as baseline material for IFMOS resulting in high structural and thermal stability and low mass. Up to now C/SiC has been demonstrated for low mass mirrors up to 60 cm and OGSE structural elements up to 2m. For NGST use the following parameters need to be verified:

- optical figure of C/SiC mirrors at RT and operational temperature as well as after vibration testing
- straylight properties (surface quality) for large mirrors

. stability of C/SiC interface connections (with C/SiC and other materials)

The following **technology pre-development** activities are proposed. *These activities are considered mandatory, as prove of concept (to ensure C/SiC material applicability for low temperature):*

1. Measurement of C/SiC physical parameters down to 20K (CTE, thermal conductance, thermal capacitance, Young's modulus, strength, etc.) Duration: 6 months
2. Behavior of C/SiC mirror surface at low temperatures Duration: 12 months
  - . Manufacturing of test mirror with a typical IFMOS size (20cm)
  - . Optical performance measurements at ambient, LN2 and 20 K

The following additional **technology developments** are aiming to gain further experience with this material:

3. Joining of interface elements Duration: 8 months
  - . Manufacturing of test plates with selected candidate joining methods
  - . Load and stability tests at RT, thermo-stability at LN2 and 20 K
4. Opto-mechanical performance at low temperatures Duration: 12 months
  - . Manufacturing of test cube of typical IFMOS size (1m X 1m x 1m)
  - . Opto-mechanical performance from ambient down to LN2 (extrapolation to 30K)

## 12.2.2 Verification of image slicer opto-mechanical concept

Current image slicer prototyping activities concentrate on optical performance of selected slices. The space compatibility of the current baseline concept should also be verified prior to further design activities:

- . optical performance of representative slicer unit
- . thermal stability down to 30 K
- . vibration stability at launch conditions and stability after thermal cycling

*As for the C/SiC material, the following **technology pre-development** activities are considered mandatory to ensure the image slicer concept feasibility for low temperature application:*

1. Critical review of the present prototype design and measured performance
2. Manufacturing and performance testing of a representative AI image slicer (72 slices) at RT and 30K
3. Design improvement incl. material review/selection

Duration 12 months

The following further **technology development** activities are recommended to gain experience with the image slicer technology:

4. manufacturing of an engineering model (representative in all critical areas)
5. verification of performance
  - . prior to and after thermal cyclings
  - . prior to and after static and vibration loads

at ambient and operational conditions

Duration 15 months

## 13 DEVELOPMENT PLANNING FOR PHASE B AND C/D

### 13.1 WORK BREAKDOWN STRUCTURE

The function oriented Work Breakdown Structure (WBS) is shown in Figure 42 below. The project is subdivided in management, product assurance, engineering, MAIT and procurement tasks. This WBS and the hardware tree shown in Figure 42 form the basis for the cost estimates.

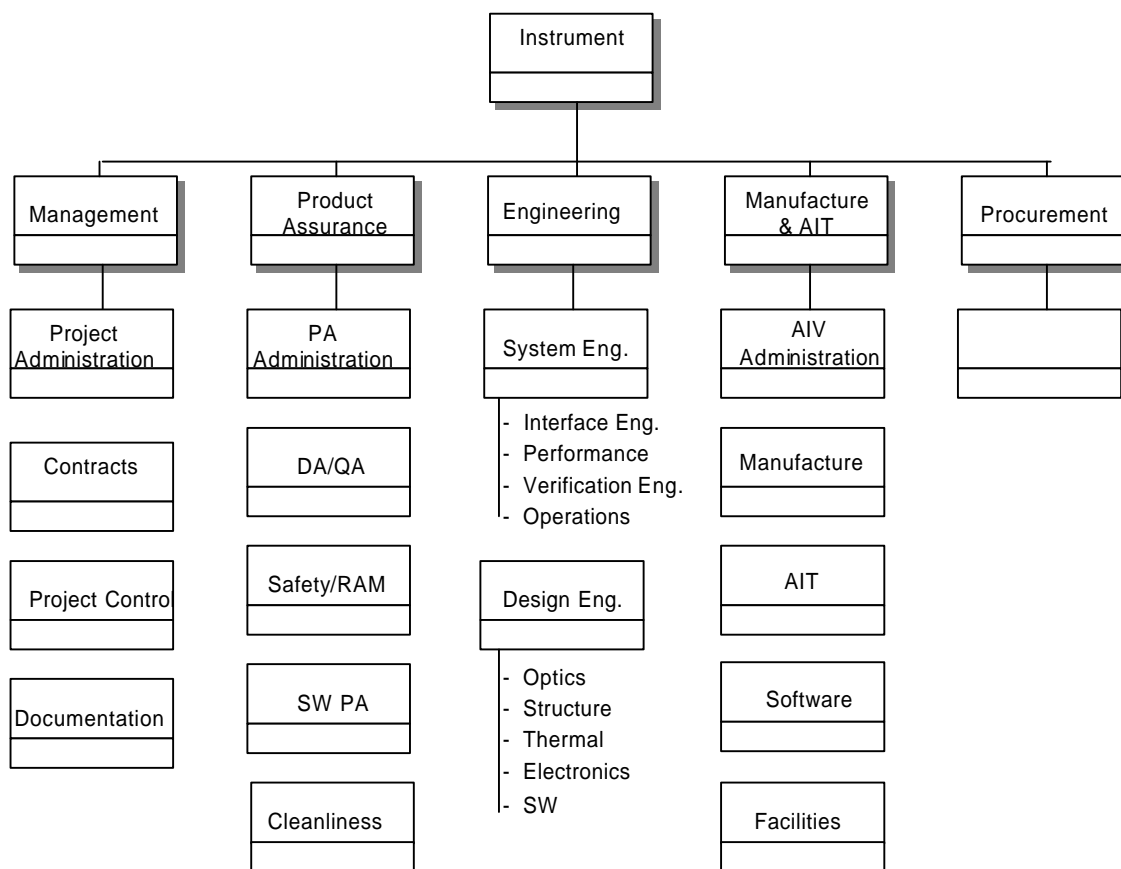


**Figure 42 : Function oriented Work Breakdown Structure**

## 13.2 DEVELOPMENT PLANNING

### 13.2.1 Model Philosophy and Schedule Planning

Two model philosophies have been considered:

#### Standard Model Philosophy and Schedule

This philosophy is based on a standard (European) space project approach, aiming at low risk ( Figure 43). The development risk is minimized by building a set of prototypes and models which are used to identify potential risks for the flight model. Besides technology breadboards and protortypes the following models are envisaged:

- . Structural/Thermal Model (STM)
- . Engineering Qualification Model (EQM)
- . Flight Model (FM)
- . Flight Spare

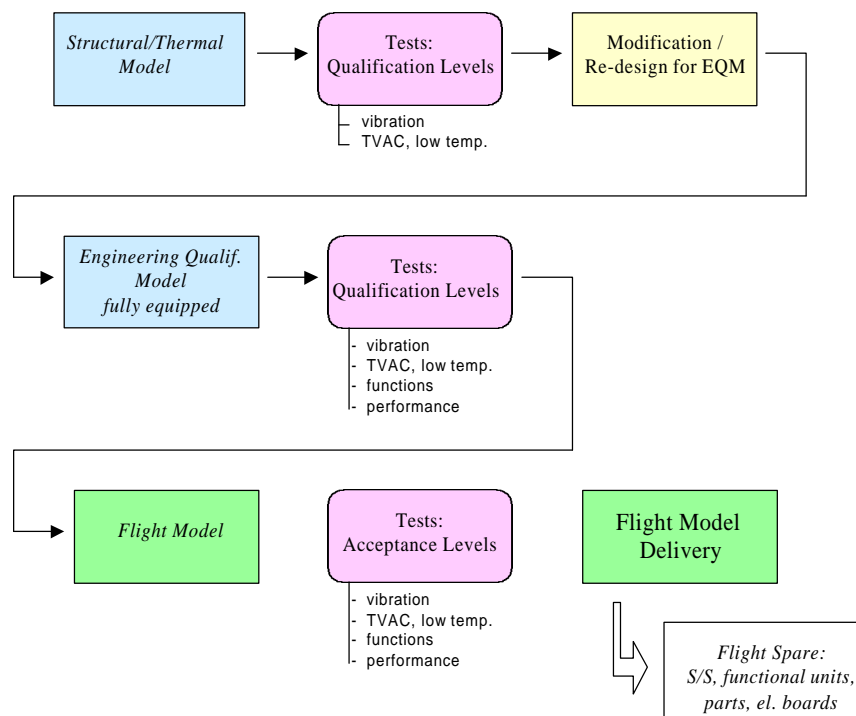


**Figure 43 : Standard Model Philosophy**

With the STM the structural and thermal performance at low temperatures and after launch loads is verified. Possible design modifications for the EQM will be derived. The STM will then be shipped to NASA for system level tests.

The EQM will be fully equipped and will undergo all performance and environmental tests on qualification levels. Design modifications for the FM will be derived, if necessary. After extensive testing the go-ahead for the FM will be given, which will be tested to acceptance levels. The flight spare will consist of a set of instrument functional units and spare parts.

The main drawback of this approach is the long development duration: the FM delivery will not be before end of 2007, see Figure 44. This delivery date is about 1.5 years later than scheduled by NASA.

The advantage of this approach is the identification of hardware problems at the earliest possible stages. This will allow to implement design modifications and reduce the risk for the flight model performance.

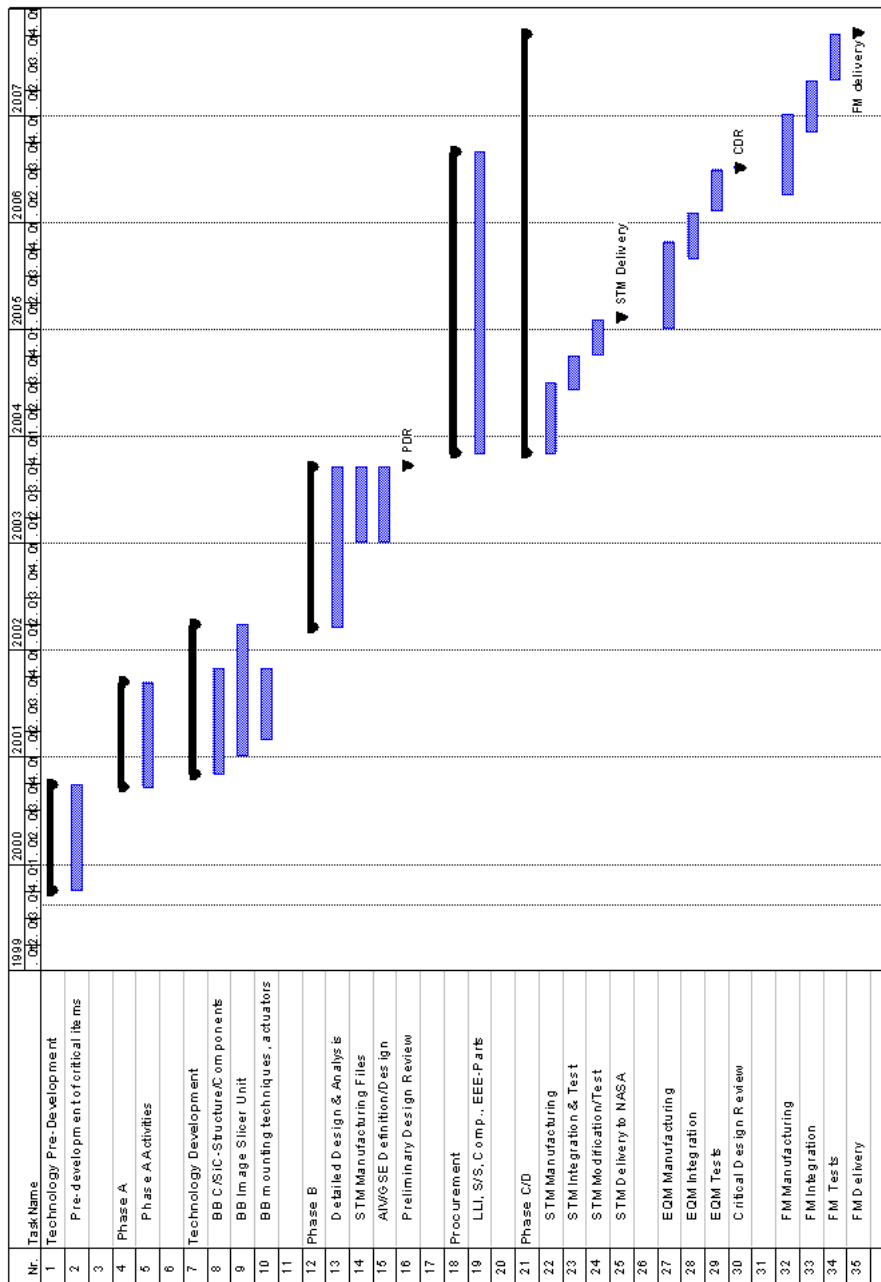


**Figure 44 : Proposed Development Schedule for Standard Model Philosophy**

### Alternative Model Philosophy and schedule

In order to meet the NASA need dates for IFMOS the above presented „standard“ schedule has to be reduced in time. This will lead to a reduction of models and will increase the risk. Besides technology breadboards and prototypes the following models are proposed:

- Structural/Thermal Model (STM)
- Demonstration Model (DM)
- Proto-Flight Model (PFM)
- Flight Spare

The alternative model philosophy is shown Figure 45 below.

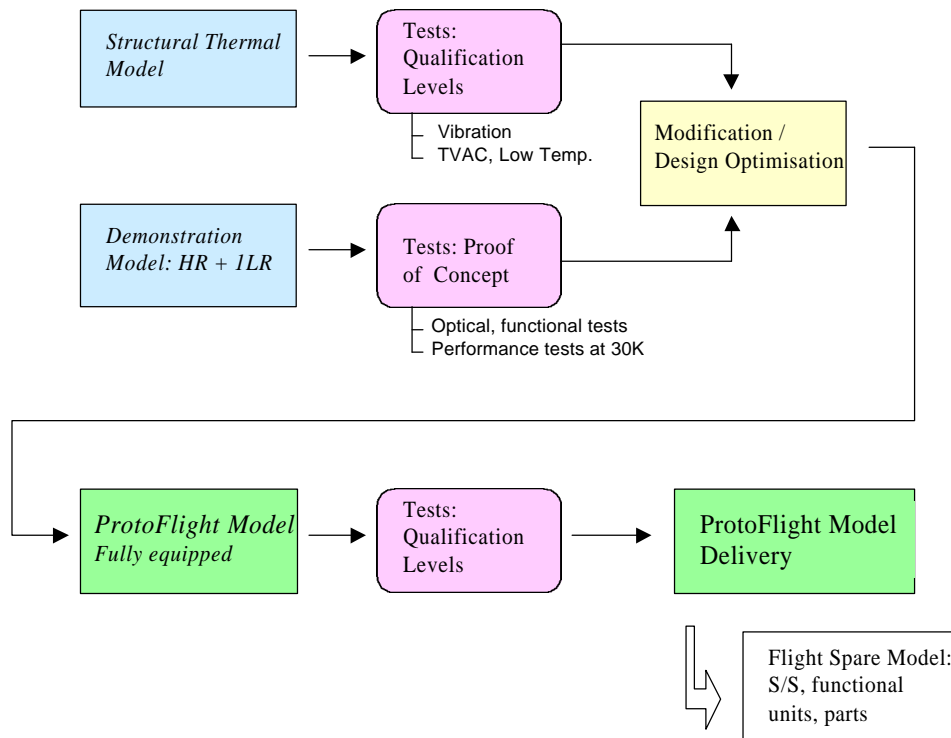


**Figure 45:** Alternative Model Philosophy

Even with a reduced development program the STM is still considered mandatory to verify the performance of the large instrument structure at the low operating temperatures and after launch loads. After testing the STM will be shipped to NASA for system level tests.

In parallel to the STM a DM will be equipped with the HR optical channel and one LR optical channel for the opto-mechanical verification of the concept. The DM will undergo an accelerated performance and environmental test program. Both the STM and the DM test results will then be used to identify design improvements for the PFM.

The PFM will be the first fully equipped instrument, and will be tested at qualification levels. The flight spare will consist of a set of instrument functional units and spare parts.

The major drawback of this approach is that the first real and complete optical verification of the instrument will be performed on PFM level and that the final impacts of structural/ thermal and opto-mechanical modifications can not be clarified before PFM availability. Any unforeseeable technical problems discovered at PFM level may lead to significant schedule delays.

Although with this alternative approach the associated risk is higher than for the standard model philosophy, it nevertheless bears the potential to meet the requested NASA need dates.

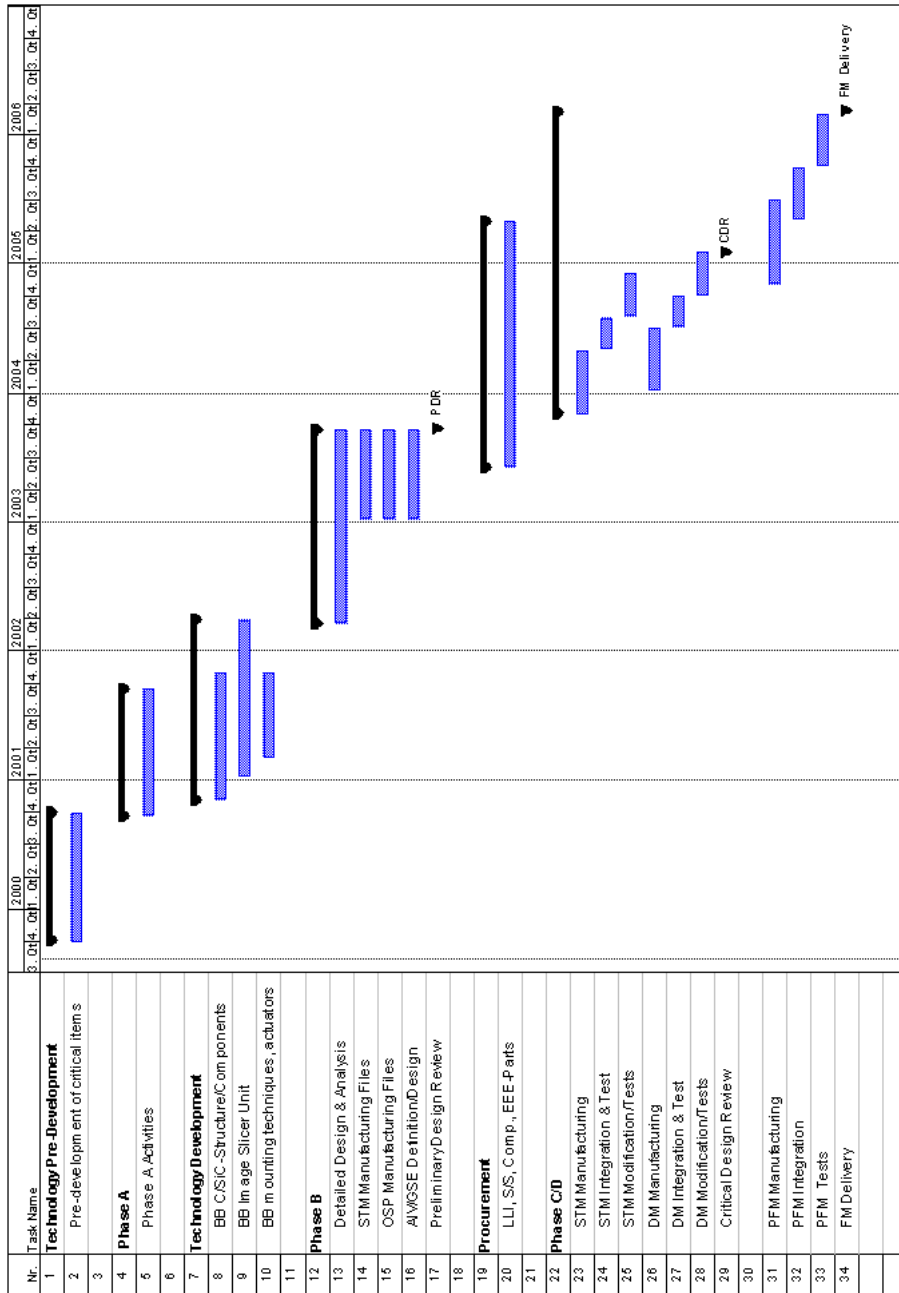


Figure 46: Proposed Development Schedule for the Alternative Model Philosophy

## 14 SUMMARY AND CONCLUSIONS

During the course of this ESA study, we have identified a concept for near infrared spectroscopy with the NGST, and we have conducted a detailed design of the instrument meeting all the requirements for the NGST instrument payload. We are proposing a spectrograph with 2 modes, a wide field survey mode, and a narrow field high resolution mode, operating simultaneously. A spectrograph with these combined modes of operation will very efficiently carry all of the proposed programs in the Design Reference Mission.

Science requirements indicate that spatially resolved spectroscopy is critically needed for a broad range of science programs. Integral field spectroscopy will be required to solve complex astrophysical issues. Performances estimates show that this spectrograph can reach the faintest levels for single objects (ultimate performance), and will provide a unique capability to conduct survey-type observations.

We have successfully conducted the following activities:

- . Review of the science requirements for spectroscopy in the 1-5 microns domain
- . Concept trade-off to select the most promising integral field spectroscopy concept: a multi-modules spectrograph fed by an image slicer unit
- . Optical design of the low resolution and high resolution spectrographs
- . Optical design of the image slicer and fore-optics
- . Mechanical, Thermal and Electrical Design and Analysis
- . Critical Areas, development Needs and follow-on activities
- . Development planning
- . Costing (kept confidential with ESA)

The results of this study demonstrate that an integral field spectrograph is both required by the science and technically feasible with limited development needs, and low technical risk.

We conclude that an integral field spectrograph should definitely be part of the NGST instrument payload .